

THE FRACTIONAL VIRIAL POTENTIAL ENERGY IN TWO-COMPONENT SYSTEMS

R. Caimmi and T. Valentinuzzi

*Dipartimento di Astronomia, Università di Padova
Vicolo Osservatorio 2, I-35122 Padova, Italy*

E-mail: roberto.caimmi@unipd.it, tiziano.valentinuzzi@unipd.it

(Received: May 17, 2008; Accepted: June 4, 2008)

SUMMARY: Two-component systems are conceived as macrogases, and the related equation of state is expressed using the virial theorem for subsystems, under the restriction of homeoidally striated density profiles. Explicit calculations are performed for a useful reference case and a few cases of astrophysical interest, both with and without truncation radius. Shallower density profiles are found to yield an equation of state, $\phi = \phi(y, m)$, characterized (for assigned values of the fractional mass, $m = M_j/M_i$) by the occurrence of two extremum points, a minimum and a maximum, as found in an earlier attempt. Steeper density profiles produce a similar equation of state, which implies that a special value of m is related to a critical curve where the above mentioned extremum points reduce to a single horizontal inflexion point, and curves below the critical one show no extremum points. The similarity of the isofractional mass curves to van der Waals' isothermal curves, suggests the possibility of a phase transition in a bell-shaped region of the $(Oy\phi)$ plane, where the fractional truncation radius along a selected direction is $y = R_j/R_i$, and the fractional virial potential energy is $\phi = (E_{ji})_{\text{vir}}/(E_{ij})_{\text{vir}}$. Further investigation is devoted to mass distributions described by Hernquist (1990) density profiles, for which an additional relation can be used to represent a sample of $N = 16$ elliptical galaxies (EGs) on the $(Oy\phi)$ plane. Even if the evolution of elliptical galaxies and their hosting dark matter (DM) haloes, in the light of the model, has been characterized by equal fractional mass, m , and equal scaled truncation radius, or concentration, $\Xi_u = R_u/r_u^\dagger$, $u = i, j$, still it cannot be considered as strictly homologous, due to different values of fractional truncation radii, y , or fractional scaling radii, $y^\dagger = r_j^\dagger/r_i^\dagger$, deduced from sample objects.

Key words. Galaxies: evolution – dark matter – Galaxies: halos

1. INTRODUCTION

Ordinary fluids (e.g., gases and liquids) may be bounded by rigid walls which allow particle number conservation, avoiding evaporation. Macroscopical parameters (pressure, density, and temperature) remain uniform within the box, due to its reduced

dimensions. On the other hand, astrophysical fluids (e.g., stars and galaxies) may be conceived as bounded by "gravitational" walls which violate particle number conservation by allowing evaporation. The macroscopical parameters exhibit gradients because they cannot remain uniform within the "gravitational" box, due to its large-scale dimensions.

In particular, sufficiently extended celestial objects show at least two distinct components: core-envelope for stars, core-halo for elliptical galaxies, bulge-disk for spiral and lenticular galaxies, baryonic-nonbaryonic for virialized (matter) density perturbations, and matter-dark energy for virialized (matter + dark energy) density perturbations. On this basis, an investigation on two-component astrophysical fluids appears useful for the comprehension and the interpretation of what is inferred from observations. To this aim, the choice of the density profiles is of basic importance. The laws of ideal and real gases were deduced from ordinary fluids, characterized by uniform density profiles. Accordingly, it is expected that astrophysical fluid laws are related to the specified density profiles, and different laws hold for different matter distributions.

Strictly speaking, a density profile should be deduced from the distribution function, or vice versa. Unfortunately, the determination of the distribution function is much more difficult than in one-component systems, and only a few cases have been studied in detail at present (e.g. Ciotti 1996, 1999). On the other hand, global properties exhibited by simple density profiles (with somewhere negative distribution function) are expected to maintain a similar trend in dealing with much more complex density profiles (with nonnegative distribution function).

As the current attempt is mainly aimed to explore global properties instead of local properties, density profiles shall be selected according to their intrinsic simplicity, regardless from the physical meaning of the distribution function. Configurations described by simple density profiles could be sufficiently close to their counterparts described by self-consistent density profiles, and the related results hold as a first approximation. In any case, the self-consistency of density profiles with respect to nonnegativity of the distribution function, can be checked using a specific theorem (Ciotti and Pellegrini 1992).

To this approximation, the particle number shall be assumed conserved, which is equivalent to conceiving the boundary of each subsystem as a perfectly reflecting surface in order to avoid evaporation. In this view, a possible choice of macroscopical parameters is: the fractional virial potential energy ϕ ; the fractional truncation radius y ; and the fractional mass m ; as was done in a pioneering paper dealing with uniform density profiles i.e. homogeneous configurations (Caimmi and Secco 1990, hereafter quoted as CS90). Accordingly, each subsystem is assumed virialized, in the sense that the virial equations are satisfied by averaging over a sufficiently long time, and particles move within a bounded region (e.g. Landau and Lifchitz 1966, Chap. II, §10; Caimmi 2007a). Then virial equilibrium is a necessary (but not sufficient) condition for dynamic or hydrostatic equilibrium, which, on the other hand, does not imply pressureless configurations, as the stress tensor is related to the kinetic-energy tensor (e.g. Binney and Tremaine 1987, Chap. 4, §2).

For sake of simplicity, the applications of the general theory shall be restricted to homeoidally stri-

ated density profiles (e.g. Roberts 1962, Caimmi 1993, Caimmi and Marmo 2003, hereafter quoted as CM03). The larger effects of asphericity are expected to occur in homogeneous configurations, which have widely been investigated (Brosche et al. 1983, Caimmi et al. 1984, CS90, Caimmi and Secco 1992). Focally striated density profiles involve far larger difficulty (e.g. Caimmi 1995, 2003).

The current investigation is mainly devoted to the following points: (i) expression of an equation of state for two-component systems; (ii) description of global properties deduced from selected density profiles; and (iii) application to elliptical galaxies belonging to a restricted sample, to be represented on the $(Oy\phi)$ plane, for fiduciary values of model parameters.

The work is organized as follows. The basic theory of two-component systems with homeoidally striated density profiles is reviewed and extended (to include both cored and cuspy matter distributions) in Section 2. The particularization to selected density profiles, involving explicit expressions, is given in Section 3. The results and related global properties are described and discussed in Section 4. Elliptical galaxies belonging to a restricted sample, are represented on the $(Oy\phi)$ plane, for fiduciary values of model parameters, in Section 5, where some considerations are given. The concluding remarks are reported in Section 6.

2. BASIC THEORY

A general theory of two-component matter distributions has been exhaustively treated in an earlier paper (Caimmi and Secco 1992), and the interested reader is addressed therein and in parent investigations (MacMillan 1930, Chap. III, §76, Limber 1959, Neutsch 1979, Brosche et al. 1983, Caimmi et al. 1984) for further details. What is relevant for the current attempt, shall be reviewed and extended. If not otherwise stated, matter distributions should be conceived as continuous media instead of discrete particle sets (e.g. Limber 1959, Caimmi 2007a). In the following, general definitions and related explicit expressions will be provided. Readers mainly interested to a simple reference case and a few cases of astrophysical interest, might directly go to Section 3, while readers mainly interested to the results and an application to elliptical galaxies, might directly go to Sections 4 and 5, respectively.

2.1. Kinetic-energy and self potential-energy tensors

Throughout the current paper, 3×3 tensors, T_{pq} , shall be dealt with, ($p = 1, 2, 3$ and $q = 1, 2, 3$). To gain space, this circumstance shall be omitted in the forthcoming formulae.

For any selected density profile, the kinetic-energy tensor and the kinetic energy read (Binney and Tremaine 1987, Chap. 4, §4.3):

$$(E_{\text{kin}})_{pq} = \frac{1}{2} \int_S \rho(x_1, x_2, x_3) v_p v_q d^3 S ; \quad (1a)$$

$$E_{\text{kin}} = \frac{1}{2} \int_S \rho(x_1, x_2, x_3) \sum_{s=1}^3 v_s^2 d^3 S ; \quad (1b)$$

while the self potential-energy tensor and the self potential energy read (Chandrasekhar 1969, Chap. 2, §10):

$$\begin{aligned} (E_{\text{sel}})_{pq} &= \int_S \rho(x_1, x_2, x_3) x_p \frac{\partial \mathcal{V}}{\partial x_q} d^3 S \\ &= -\frac{1}{2} \int_S \rho(x_1, x_2, x_3) \mathcal{V}_{pq}(x_1, x_2, x_3) d^3 S ; \end{aligned} \quad (2a)$$

$$\begin{aligned} E_{\text{sel}} &= \int_S \rho(x_1, x_2, x_3) \sum_{s=1}^3 x_s \frac{\partial \mathcal{V}}{\partial x_s} d^3 S \\ &= -\frac{1}{2} \int_S \rho(x_1, x_2, x_3) \mathcal{V}(x_1, x_2, x_3) d^3 S ; \end{aligned} \quad (2b)$$

where ρ is the density, $d^3 S = dx_1 dx_2 dx_3$ is an infinitesimal volume element placed at $\mathbf{P} = (x_1, x_2, x_3)$, $v_p v_q = \overline{v_p v_q}$ and $v_s^2 = \overline{(v_s^2)}$ are arithmetic means calculated within $d^3 S$, \mathcal{V}_{pq} and \mathcal{V} are the gravitational tensor potential and potential, respectively (Chandrasekhar 1969, Chap. 2, §10):

$$\begin{aligned} \mathcal{V}_{pq}(x_1, x_2, x_3) &= G \int_S \rho(x'_1, x'_2, x'_3) \\ &\quad \times \frac{(x'_p - x_p)(x'_q - x_q)}{|\vec{R} - \vec{R}'|^3} d^3 S' ; \end{aligned} \quad (3a)$$

$$\mathcal{V}(x_1, x_2, x_3) = G \int_S \rho(x'_1, x'_2, x'_3) \frac{d^3 S'}{|\vec{R} - \vec{R}'|} ; \quad (3b)$$

where G is the gravitation constant, $\vec{R} = \overline{\mathbf{OP}}$ and $\vec{R}' = \overline{\mathbf{OP}'}$, $\mathbf{P}' = (x'_1, x'_2, x'_3)$, radius vectors with origin at the centre of inertia.

In accordance with Eq. (3), the normalization of the potential satisfies the boundary condition to be null at infinite distances, and then positive elsewhere (e.g. MacMillan 1930, Chap. II, §20, Chandrasekhar 1969, Chap. 3, §17, Caimmi and Secco 2003), rather than null at the centre of inertia, and negative elsewhere (e.g. Binney and Tremaine 1987, Chap. 2, §1, Mouri and Taniguchi 2003).

Let i and j denote the subsystems of a two-component matter distribution. The potential-energy tensor and the potential energy may be cast into the form (Caimmi and Secco 1992):

$$(E_{\text{pot}})_{pq} = [(E_i)_{\text{sel}}]_{pq} + [(E_{ij})_{\text{int}}]_{pq} + [(E_{ji})_{\text{int}}]_{pq} + [(E_j)_{\text{sel}}]_{pq} ; \quad (4a)$$

$$E_{\text{pot}} = (E_i)_{\text{sel}} + (E_{ij})_{\text{int}} + (E_{ji})_{\text{int}} + (E_j)_{\text{sel}} ; \quad (4b)$$

where the expression for the potential energy (e.g. MacMillan 1930, Chap. III, §76) has been generalized to the potential-energy tensor; in addition, the interaction potential-energy tensor, $[(E_{uv})_{\text{int}}]_{pq}$, and the interaction potential energy, $(E_{uv})_{\text{int}}$, read:

$$\begin{aligned} [(E_{uv})_{\text{int}}]_{pq} &= -\frac{1}{2} \int_{S_u} \rho_u(x_1, x_2, x_3) [\mathcal{V}_v(x_1, x_2, x_3)]_{pq} \\ &\quad \times d^3 S ; \quad u = i, j ; \quad v = j, i ; \end{aligned} \quad (5a)$$

$$\begin{aligned} (E_{uv})_{\text{int}} &= -\frac{1}{2} \int_{S_u} \rho_u(x_1, x_2, x_3) \mathcal{V}_v(x_1, x_2, x_3) d^3 S ; \\ u &= i, j ; \quad v = j, i ; \end{aligned} \quad (5b)$$

which are symmetric with respect to the exchange of one component with the other:

$$[(E_{ij})_{\text{int}}]_{pq} = [(E_{ji})_{\text{int}}]_{pq} ; \quad (6a)$$

$$(E_{ij})_{\text{int}} = (E_{ji})_{\text{int}} ; \quad (6b)$$

for further details refer to earlier attempts (MacMillan 1930, Chap. III, §76, Caimmi and Secco 1992).

To gain space, the relations, $u = i, j$, $v = j, i$, which mean u, v are generic subsystems while i, j are the inner and the outer one, respectively, shall be omitted in the forthcoming formulae.

The tidal potential-energy tensor and the tidal potential energy read (e.g. Caimmi and Secco 1992):

$$[(E_{uv})_{\text{tid}}]_{pq} = \int_{S_u} \rho_u(x_1, x_2, x_3) x_p \frac{\partial \mathcal{V}_v}{\partial x_q} d^3 S ; \quad (7a)$$

$$(E_{uv})_{\text{tid}} = \int_{S_u} \rho_u(x_1, x_2, x_3) \sum_{s=1}^3 x_s \frac{\partial \mathcal{V}_v}{\partial x_s} d^3 S ; \quad (7b)$$

where the tidal potential energy, $(E_{uv})_{\text{tid}}$, may be conceived as the virial of the u -th component in connection with the tidal field induced by the v -th component (Brosche et al. 1983).

The tensor and the scalar virial theorem for a single subsystem, within the tidal field induced by the other one, read (Caimmi et al. 1984, Caimmi and Secco 1992):

$$2[(E_u)_{\text{kin}}]_{pq} + [(E_u)_{\text{sel}}]_{pq} + [(E_{uv})_{\text{tid}}]_{pq} = 0 ; \quad (8a)$$

$$2(E_u)_{\text{kin}} + (E_u)_{\text{sel}} + (E_{uv})_{\text{tid}} = 0 ; \quad (8b)$$

which is the generalization of previous results related to one-component systems (e.g. Chandrasekhar 1969, Chap. II, §11, Binney and Tremaine 1987, Chap. 4, §3). The validity of the relations (Caimmi and Secco 1992):

$$\begin{aligned} [(E_{ij})_{\text{tid}}]_{pq} + [(E_{ji})_{\text{tid}}]_{pq} &= [(E_{ij})_{\text{int}}]_{pq} \\ &\quad + [(E_{ji})_{\text{int}}]_{pq} ; \end{aligned} \quad (9a)$$

$$(E_{ij})_{\text{tid}} + (E_{ji})_{\text{tid}} = (E_{ij})_{\text{int}} + (E_{ji})_{\text{int}} ; \quad (9b)$$

implies the following:

$$[(E_{uv})_{\text{tid}}]_{pq} = [(E_{uv})_{\text{int}}]_{pq} + [(E_{uv})_{\text{res}}]_{pq} ; \quad (10a)$$

$$(E_{uv})_{\text{tid}} = (E_{uv})_{\text{int}} + (E_{uv})_{\text{res}} ; \quad (10b)$$

where $[(E_{uv})_{\text{res}}]_{pq}$ and $(E_{uv})_{\text{res}}$ are the residual potential-energy tensor and the residual potential energy, respectively, which are antisymmetric with respect to the exchange of one component with the other:

$$[(E_{ij})_{\text{res}}]_{pq} = -[(E_{ji})_{\text{res}}]_{pq} ; \quad (11a)$$

$$(E_{ij})_{\text{res}} = -(E_{ji})_{\text{res}} ; \quad (11b)$$

for further details refer to earlier attempts (Caimmi and Secco 1992, Caimmi 2007b).

It can be seen from Eqs. (6), (10), and (11), that the tidal potential-energy tensor, $[(E_{uv})_{\text{tid}}]_{pq}$, and the tidal potential energy, $(E_{uv})_{\text{tid}}$, are made of a symmetric term, $[(E_{uv})_{\text{int}}]_{pq}$ and $(E_{uv})_{\text{int}}$, and an antisymmetric one, $[(E_{uv})_{\text{res}}]_{pq}$ and $(E_{uv})_{\text{res}}$, respectively, with respect to the exchange of one component with the other.

The virial theorem in tensor and in scalar form, expressed by Eqs. (8), may be written in more compact form:

$$2[(E_u)_{\text{kin}}]_{pq} + [(E_{uv})_{\text{vir}}]_{pq} = 0 ; \quad (12a)$$

$$2(E_u)_{\text{kin}} + (E_{uv})_{\text{vir}} = 0 ; \quad (12b)$$

where the virial potential-energy tensor, $[(E_{uv})_{\text{vir}}]_{pq}$, and the virial potential energy, $(E_{uv})_{\text{vir}}$, are defined as:

$$[(E_{uv})_{\text{vir}}]_{pq} = [(E_u)_{\text{sel}}]_{pq} + [(E_{uv})_{\text{tid}}]_{pq} ; \quad (13a)$$

$$(E_{uv})_{\text{vir}} = (E_u)_{\text{sel}} + (E_{uv})_{\text{tid}} ; \quad (13b)$$

where, in general, the virial potential energy is usually named "the virial of the system" (Clausius 1870). In the case under discussion, the "system" relates to the u -th component within the tidal potential induced by the v -th component.

For the assigned density profiles, the virial potential-energy tensor and the virial energy of each subsystem can be determined, together with their kinetic counterparts via Eqs. (12a) and (12b), respectively, which constrain, in turn, the orbital anisotropy on each subsystem. More specifically, the sum of mean orbital kinetic-energy tensor and kinetic energy, has to reproduce $[(E_u)_{\text{kin}}]_{pq}$ and $(E_u)_{\text{kin}}$, respectively.

When a system is not entirely contained within its truncation radius, the usual form of the virial theorem, $2E_{\text{kin}} + E_{\text{pot}} = 0$, should be extended as $2E_{\text{kin}} + E_{\text{pot}} = 3pS$, where the last is a surface term (e.g. The and White 1986, Carlberg et al. 1996, Girardi et al. 1998). In dealing with a specified subsystem, it shall be understood that no mass exists outside the mentioned truncation radius, which makes a null surface term.

To avoid the determination of the gravitational potential, which is the most difficult step towards an explicit expression of the potential-energy tensors and potential energies, a particular procedure shall be followed under the restrictive assumption of homeoidally striated density profiles (Roberts 1962).

2.2. Homeoidally striated density profiles

Let the isopycnic (i.e. constant density) surfaces be defined by the following law (CM03):

$$\rho = \rho^\dagger f(\xi) ; \quad f(1) = 1 ; \quad (14a)$$

$$\xi^2 = \sum_{\ell=1}^3 \frac{x_\ell^2}{(a_\ell^\dagger)^2} ; \quad 0 \leq \xi \leq \Xi ; \quad (14b)$$

where $\rho^\dagger = \rho(1)$, a_ℓ^\dagger , are the density and the semi-axes, respectively, of a reference isopycnic surface, and Ξ corresponds to the truncation isopycnic surface, related to semi-axes, a_ℓ . The scaled radial coordinate, ξ , and the scaled density, f , may be conceived as the generalization of their counterparts related to polytropes (e.g. Chandrasekhar 1939, Chap. IV, §4, Horedt 2004, Chap. 2, §2.1).

According to Eqs. (14), the scaling density, ρ^\dagger , and the scaling radius, r^\dagger , correspond to a single boundary, which allows the description of both cored and cuspy density profiles. The assumption that the system is homeoidally striated implies the relation (CM03):

$$\xi = \frac{r}{r^\dagger} ; \quad (15)$$

and, in particular:

$$\Xi = \frac{R}{r^\dagger} ; \quad (16)$$

which, in any case, is independent of the radial coordinate, r , of the generic point on the selected isopycnic surface.

2.3. Mass and inertia tensor

The function (Roberts 1962):

$$F(\xi) = 2 \int_\xi^\Xi f(\xi') \xi' d\xi' ; \quad (17a)$$

$$F(\Xi) = 0 ; \quad \frac{dF}{d\xi} = -2\xi f(\xi) ; \quad (17b)$$

$$\int_0^\Xi f(\xi) \xi^n d\xi = \frac{n-1}{2} \int_0^\Xi F(\xi) \xi^{n-2} d\xi ; \quad n > 1 ; \quad (17c)$$

allows the calculation of the total mass as (CM03):

$$M = \nu_{\text{mas}} M^\dagger ; \quad (18a)$$

$$\nu_{\text{mas}} = \frac{3}{2} \int_0^\Xi F(\xi) d\xi ; \quad (18b)$$

$$M^\dagger = \frac{4\pi}{3} \rho^\dagger a_1^\dagger a_2^\dagger a_3^\dagger ; \quad (18c)$$

and the inertia tensor as (CM03):

$$I_{pq} = \delta_{pq} \nu_{\text{inr}} M^\dagger (a_p^\dagger)^2 ; \quad (19a)$$

$$\nu_{\text{inr}} = \frac{3}{2} \int_0^\Xi F(\xi) \xi^2 d\xi ; \quad (19b)$$

where the coefficients, ν_{mas} and ν_{inr} , are shape-independent and may be conceived as profile factors (Caimmi 1993), and δ_{pq} is the Kronecker symbol. For a different formulation of the inertia tensor refer to earlier attempts (e.g. Landau and Lifchitz 1966, Chap. VI, §32, Bett et al. 2007).

The mass within an isopycnic surface, $\rho = \rho^\dagger f(\xi)$, is $M(\xi) = \nu_{\text{mas}}(\xi)M^\dagger$, where $\nu_{\text{mas}}(\xi)$ is expressed by Eq. (18b) with ξ instead of Ξ . The related mean density is $\bar{\rho}(\xi) = M(\xi)/S(\xi)$, where $S(\xi)$ is the volume bounded by the isopycnic surface.

2.4. Potential-energy tensors and potential energies

The self potential-energy tensor and the self potential energy read (CM03):

$$(E_{\text{sel}})_{pq} = -\delta_{pq}\nu_{\text{sel}}\frac{G(M^\dagger)^2}{a_1^\dagger}B_p ; \quad (20a)$$

$$E_{\text{sel}} = -\nu_{\text{sel}}\frac{G(M^\dagger)^2}{a_1^\dagger}B ; \quad (20b)$$

$$\nu_{\text{sel}} = \frac{9}{16}\int_0^\Xi F^2(\xi) d\xi ; \quad (20c)$$

$$B_p = \epsilon_{p2}\epsilon_{p3}\int_0^{+\infty}(1+s')^{-3/2}(1+\epsilon_{pq}^2s')^{-1/2} \\ \times (1+\epsilon_{pr}^2s')^{-1/2} ds' ; \quad (20d)$$

$$B = \sum_{s=1}^3 B_p ; \quad \epsilon_{mn} = \frac{a_m}{a_n} ; \quad (20e)$$

where ν_{sel} is a profile factor, ϵ_{mn} are axis ratios, and B_p are shape factors which, *ipso facto*, depend on the axis ratios only (Caimmi 1992).

The above results are related to a single subsystem: strictly speaking, all the quantities defined in the current section should be labelled by the index, u , indicating connection with the u -th subsystem (e.g. Caimmi and Secco 1992), but it has been omitted to gain clarity. On the other hand, the formulation of other potential-energy tensors and potential energies necessarily involves (at least) two components. The related calculations are very difficult in the general case, and for this reason only the special situation of similar and similarly placed boundaries shall be considered.

With this restriction, the combination of Eqs. (15), (16), and (18c), related to both density profiles, the inner one be denoted by i and the outer by j , yields:

$$\xi_i = y^\dagger \xi_j ; \quad \frac{\Xi_j}{\Xi_i} = \frac{y}{y^\dagger} ; \quad \frac{(\nu_j)_{\text{mas}}}{(\nu_i)_{\text{mas}}} = \frac{m}{m^\dagger} ; \quad (21a)$$

$$y = \frac{R_j}{R_i} ; \quad y^\dagger = \frac{r_j^\dagger}{r_i^\dagger} ; \quad m = \frac{M_j}{M_i} ; \quad m^\dagger = \frac{M_j^\dagger}{M_i^\dagger} ; \quad (21b)$$

which allows to express the other potential-energy

tensors and potential energies, as (CM03):

$$[(E_{uv})_{\text{xxx}}]_{pq} = -\delta_{pq}\frac{G(M_u^\dagger)^2}{(a_u^\dagger)_1}(\nu_{uv})_{\text{xxx}}B_p ; \quad (22a)$$

$$(E_{uv})_{\text{xxx}} = -\frac{G(M_u^\dagger)^2}{(a_u^\dagger)_1}(\nu_{uv})_{\text{xxx}}B ; \quad (22b)$$

$$u = i, j ; \quad v = j, i ; \quad \text{xxx} = \text{int, tid, res, vir} ; \quad (22c)$$

and the explicit expression of the profile factors reads (CM03):

$$(\nu_{ij})_{\text{int}} = -\frac{9}{16}m^\dagger \left[w^{(\text{int})}(\eta) + w^{(\text{ext})}(\eta) \right] ; \quad (23a)$$

$$(\nu_{ij})_{\text{tid}} = -\frac{9}{8}m^\dagger w^{(\text{ext})}(\eta) ; \quad (23b)$$

$$(\nu_{ji})_{\text{tid}} = -\frac{9}{8}\frac{y^\dagger}{m^\dagger}w^{(\text{int})}(\eta) ; \quad (23c)$$

$$(\nu_{ij})_{\text{res}} = -\frac{9}{16}m^\dagger \left[w^{(\text{int})}(\eta) - w^{(\text{ext})}(\eta) \right] ; \quad (23d)$$

$$(\nu_{uv})_{\text{vir}} = (\nu_u)_{\text{sel}} + (\nu_{uv})_{\text{tid}} ; \quad (23e)$$

$$(\nu_{ij})_{\text{int}} = (\nu_{ji})_{\text{int}} ; \quad (\nu_{ij})_{\text{res}} = -(\nu_{ji})_{\text{res}} ; \quad (23f)$$

$$\eta = \frac{\Xi_i}{y^\dagger} = \frac{\Xi_j}{y} ; \quad (23g)$$

where the functions $w^{(\text{int})}$ and $w^{(\text{ext})}$ are defined as (CM03):

$$w^{(\text{int})}(\eta) = \int_0^\eta F_j(\xi_j)\frac{dF_i}{d\xi_j}\xi_j d\xi_j ; \quad (24a)$$

$$w^{(\text{ext})}(\eta) = \int_0^\eta F_i(\xi_i)\frac{dF_j}{d\xi_j}\xi_j d\xi_j ; \quad (24b)$$

in conclusion, Eqs. (20)-(24) allow to calculate the potential-energy tensors and potential energies for homeoidally striated density profiles in the presence of similar and similarly placed boundaries.

In the case under discussion, due to Eqs. (22), the fractional virial potential-energy tensor component equals the fractional virial potential energy, as:

$$\phi = \frac{[(E_{ji})_{\text{vir}}]_{pq}}{[(E_{ij})_{\text{vir}}]_{pq}} = \frac{(E_{ji})_{\text{vir}}}{(E_{ij})_{\text{vir}}} = \frac{(m^\dagger)^2}{y^\dagger} \frac{(\nu_{ji})_{\text{vir}}}{(\nu_{ij})_{\text{vir}}} ; \quad (25)$$

which, for the density profiles considered, depends on the reference fractional mass, m^\dagger , and the fractional scaling radius, y^\dagger , according to Eqs. (21)-(24). The substitution of Eqs. (21) into (25) yields:

$$\phi = \frac{m^2}{y} \frac{\Xi_j}{\Xi_i} \left[\frac{(\nu_i)_{\text{mas}}}{(\nu_j)_{\text{mas}}} \right]^2 \frac{(\nu_{ji})_{\text{vir}}}{(\nu_{ij})_{\text{vir}}} ; \quad (26)$$

which, for the density profiles considered, depends on the fractional mass, m , and the fractional truncation radius, y , according to Eqs. (21)-(24).

Strictly speaking, Eqs. (21)-(26) are valid provided the indices, i and j , denote the embedded and

the embedding subsystem, respectively, which implies $y \geq 1$. This is why the above procedure is valid only for the inner component, where the Poisson equation instead of the Laplace one holds with respect to the gravitational potential. The remaining results, related to the outer component, are obtained by use of the symmetry of the interaction potential-energy tensor and interaction potential energy, Eqs. (6), and the antisymmetry of the residual potential-energy tensor and residual potential energy, Eqs. (11).

If the role of the two subsystems is reversed, $0 \leq y \leq 1$, it has to be kept in mind that, in this case, the inner and the outer component are denoted by the indices, j and i , respectively, and the reversion must be carried out in Eqs. (21)-(26), through the following steps: (i) make the changes: $m \rightarrow m^{-1}$; $m^\dagger \rightarrow (m^\dagger)^{-1}$; $y \rightarrow y^{-1}$; $y^\dagger \rightarrow (y^\dagger)^{-1}$; $\Xi_i \leftrightarrow \Xi_j$; $(\nu_i)_{\text{mas}} \leftrightarrow (\nu_j)_{\text{mas}}$; $(\nu_i)_{\text{sel}} \leftrightarrow (\nu_j)_{\text{sel}}$; (ii) for assigned $y \geq 1$ and $y^\dagger = (\Xi_i/\Xi_j)y$, calculate the functions, $w^{(\text{int})}(\eta)$ and $w^{(\text{ext})}(\eta)$; (iii) calculate the profile factors, $(\nu_{ij})_{\text{tid}}$ and $(\nu_{ji})_{\text{tid}}$, as well as the remaining ones whenever needed; (iv) calculate the fractional virial potential energy, ϕ ; (v) make the changes, $m \rightarrow m^{-1}$; $m^\dagger \rightarrow (m^\dagger)^{-1}$; $y \rightarrow y^{-1}$; $y^\dagger \rightarrow (y^\dagger)^{-1}$; $\phi \rightarrow \phi^{-1}$; which allow the extension of the fractional virial potential energy, $\phi = (E_{ji})_{\text{vir}}/(E_{ij})_{\text{vir}}$, to the domain, $0 \leq y \leq 1$.

In absence of truncation radius, $\Xi \rightarrow +\infty$, $\eta \rightarrow +\infty$, the reversion occurs when the density drops to zero and nothing changes except in infinitesimal terms of higher order and infinite terms of lower order. Accordingly, there is no need to perform the reversion in this case.

The relation, $\phi = \phi(y^\dagger, m^\dagger)$, or its counterpart, $\phi = \phi(y, m)$, expressed by Eqs. (25) and (26), respectively, may be conceived as an equation of state for the two-component systems with assigned homeoidally striated density profiles. At the price of major complexity, it can be formulated for any kind of two-component, ideal, self-gravitating fluids, hereafter quoted as "two-component macrogases" or, more shortly, as "macrogases".

3. SPECIAL CASES

The explicit expression for the macrogases equation of state is, in general, rather cumbersome and numerical computations should be preferred to this aim. On the other hand, the procedure is conceptually simple, as the functions $w^{(\text{int})}(\eta)$ and $w^{(\text{ext})}(\eta)$, as well as the fractional virial potential energy, ϕ , may be calculated using Eqs. (20)-(26).

Aiming to provide a description of the general trend and related features, a limited number of simple possibilities shall be analysed in detail, selecting density profiles from the family:

$$f(\xi) = \frac{2^\chi}{\xi^\gamma(1+\xi^\alpha)^\chi} ; \quad \chi = \frac{\beta-\gamma}{\alpha} ; \quad (27)$$

which is defined by three parameters, (α, β, γ) . For further details refer to earlier attempts (e.g. Hernquist 1990, Zhao 1996, Caimmi and Marmo 2004, Caimmi et al. 2005, Caimmi 2006), where special cases were fully investigated.

In the following, the macrogases equation of state shall be determined for a simple but unrealistic density profile, to be taken as a reference case, and a few density profiles of astrophysical interest. The reader whose attention is mainly directed to the results and/or the astrophysical applications of the model, is free to jump directly to Section 4 and/or 5, respectively.

3.1. UU macrogases

Here, the related density profiles are uniform, $(\alpha, \beta, \gamma) = (0, 0, 0)$, and Eq. (27) reduces to:

$$f_u(\xi_u) = 1 ; \quad 0 \leq \xi_u \leq \Xi_u ; \quad u = i, j ; \quad (28)$$

which is equivalent to polytropes with index, $n = 0$ (e.g. Chandrasekhar 1939, Chap. IV, §4, Caimmi 1986) but implies unphysical situations for stellar fluids (Vandervoort 1980). The particularization of Eqs. (17a), (18b), (20c), (24a), and (24b) to the case of interest here yields:

$$F_u(\xi_u) = \Xi_u^2 - \xi_u^2 ; \quad (29)$$

$$(\nu_u)_{\text{mas}} = \Xi_u^3 ; \quad (30)$$

$$(\nu_u)_{\text{sel}} = \frac{3}{10} \Xi_u^5 ; \quad (31)$$

$$w^{(\text{int})}(\eta) = -\frac{4}{15} \Xi_i^2 \eta^3 \left(\frac{5}{2} y^2 - \frac{3}{2} \right) ; \quad (32)$$

$$w^{(\text{ext})}(\eta) = -\frac{4}{15} \Xi_i^2 \eta^3 ; \quad (33)$$

and, using Eqs. (23b), (23c) and (23g), the UU macrogases equation of state follows from the particularization of Eq. (26) to the case of interest, as:

$$\phi = \frac{(m^\dagger)^2}{y^\dagger} \left(\frac{y}{y^\dagger} \right)^5 \frac{1 + \frac{(y^\dagger)^3}{(m^\dagger)} \frac{1}{y^5} \left(\frac{5}{2} y^2 - \frac{3}{2} \right)}{1 + \frac{m^\dagger}{(y^\dagger)^3}} ; \quad (34)$$

$$y \geq 1 ;$$

and the extension of the above function to the domain, $0 \leq y \leq 1$, following the procedure outlined in Subsection 2.4, yields:

$$\phi = \left(\frac{y}{y^\dagger} \right)^5 \frac{m^\dagger (y^\dagger)^2 \left[1 + \frac{m^\dagger}{(y^\dagger)^3} \right]}{1 + m^\dagger \left(\frac{y}{y^\dagger} \right)^3 \left(\frac{5}{2} - \frac{3}{2} y^2 \right)} ; \quad (35)$$

$$0 \leq y \leq 1 ;$$

where it can be seen that in the special case, $y = 1$, Eqs. (34) and (35) do coincide. If, in addition, $\Xi_i = \Xi_j$, which implies $y^\dagger = y$, $m^\dagger = m$, via Eqs. (18) and (21), then Eqs. (34) and (35) reduce to:

$$\phi = m = m^\dagger ; \quad y = y^\dagger = 1 ; \quad (36)$$

or $\phi(1, m) = m$.

Owing to Eqs. (34) and (35), the fractional virial potential energy, ϕ , is independent of the fractional truncation radii, (Ξ_i, Ξ_j) .

3.2. PP macrogases

The related density profiles (Schuster 1883, Plummer 1911) imply $(\alpha, \beta, \gamma) = (2, 5, 0)$, and Eq. (27) reduces to:

$$f_u(\xi_u) = \frac{2^{5/2}}{(1 + \xi_u^2)^{5/2}} ; \quad 0 \leq \xi_u \leq \Xi_u ; \quad u = i, j ; \quad (37)$$

which is equivalent to polytropes with index, $n = 5$; for a formal demonstration, see Appendix 1. For one-component systems, hydrostatic equilibrium holds regardless from the nature of the fluid (Vandervoort 1980).

The particularization of Eqs. (17a), (18b), (20c), (24a), and (24b) to the case of interest yields:

$$F_u(\xi_u) = \frac{2^{7/2}}{3} \left[\frac{1}{(1 + \xi_u^2)^{3/2}} - \frac{1}{(1 + \Xi_u^2)^{3/2}} \right] ; \quad (38)$$

$$(\nu_u)_{\text{mas}} = \frac{2^{5/2} \Xi_u^3}{(1 + \Xi_u^2)^{3/2}} ; \quad (39)$$

$$(\nu_u)_{\text{sel}} = \frac{\Xi_u(3\Xi_u^4 - 8\Xi_u^2 + 13)}{(1 + \Xi_u^2)^3} + 3 \arctan \Xi_u ; \quad (40)$$

$$\begin{aligned} w^{(\text{int})}(\eta) = & -\frac{128}{3} (y^\dagger)^2 \left\{ \frac{[(y^\dagger)^2 + 7]iE(y^\dagger, i\alpha)}{3[(y^\dagger)^2 - 1]^3} + \right. \\ & + \frac{4[(y^\dagger)^2 - 1]iF(y^\dagger, i\alpha)}{3[(y^\dagger)^2 - 1]^3} + \\ & + \frac{P^{(\text{int})}(\eta, y^\dagger)}{3[(y^\dagger)^2 - 1]^3(\eta^2 + 1)[(y^\dagger)^2\eta^2 + 1]^2} - \\ & \left. - \frac{1}{(1 + \Xi_j^2)^{3/2}} \frac{\eta^3}{3[(y^\dagger)^2\eta^2 + 1]^{3/2}} \right\} ; \quad (41a) \end{aligned}$$

$$\begin{aligned} P^{(\text{int})}(\eta, y^\dagger) = & \eta\sqrt{\eta^2 + 1}\sqrt{(y^\dagger)^2\eta^2 + 1} \times \\ & \times [(y^\dagger)^6\eta^2(\eta^2 + 1) + (y^\dagger)^4\eta^2(7\eta^2 - 4) + \\ & + (y^\dagger)^2(11\eta^2 + 5) + 3] ; \quad (41b) \end{aligned}$$

$$\alpha = \text{arcsinh } \eta ; \quad y^\dagger \neq 1 ; \quad (41c)$$

$$\begin{aligned} w^{(\text{int})}(\eta) = & -\frac{128}{3} (y^\dagger)^2 \left[\frac{\arctan \eta}{16} + \right. \\ & + \frac{\eta(3\eta^4 + 8\eta^2 - 3)}{48(\eta^2 + 1)^3} - \\ & \left. - \frac{1}{(1 + \Xi_j^2)^{3/2}} \frac{\eta^3}{3(\eta^2 + 1)^{3/2}} \right] ; \\ & y^\dagger = 1 ; \quad (41d) \end{aligned}$$

$$\begin{aligned} w^{(\text{ext})}(\eta) = & -\frac{128}{3} \left\{ -\frac{[7(y^\dagger)^2 + 1]iE(y^\dagger, i\alpha)}{3[(y^\dagger)^2 - 1]^3} + \right. \\ & + \frac{[3(y^\dagger)^4 - 2(y^\dagger)^2 - 1]iF(y^\dagger, i\alpha)}{3[(y^\dagger)^2 - 1]^3} - \\ & - \frac{P^{(\text{ext})}(\eta, y^\dagger)}{3[(y^\dagger)^2 - 1]^3(\eta^2 + 1)^2[(y^\dagger)^2\eta^2 + 1]} - \\ & \left. - \frac{1}{(1 + \Xi_i^2)^{3/2}} \frac{\eta^3}{3(\eta^2 + 1)^{3/2}} \right\} ; \quad (42a) \end{aligned}$$

$$\begin{aligned} P^{(\text{ext})}(\eta, y^\dagger) = & \eta\sqrt{\eta^2 + 1}\sqrt{(y^\dagger)^2\eta^2 + 1} \times \\ & \times [(y^\dagger)^4(7\eta^4 + 11\eta^2 + 3) + \\ & + (y^\dagger)^2(\eta^4 + 4\eta^2 + 5) + \eta^2] ; \quad (42b) \end{aligned}$$

$$\alpha = \text{arcsinh } \eta ; \quad y^\dagger \neq 1 ; \quad (42c)$$

$$\begin{aligned} w^{(\text{ext})}(\eta) = & -\frac{128}{3} \left[\frac{\arctan \eta}{16} + \frac{\eta(3\eta^4 + 8\eta^2 - 3)}{48(\eta^2 + 1)^3} - \right. \\ & \left. - \frac{1}{(1 + \Xi_i^2)^{3/2}} \frac{\eta^3}{3(\eta^2 + 1)^{3/2}} \right] ; \\ & y^\dagger = 1 ; \quad (42d) \end{aligned}$$

where i is the imaginary unit, F and E are incomplete elliptic integrals of first and second kind, respectively, defined as:

$$\begin{aligned} F(k, \beta) = & \int_0^\beta \frac{d\theta}{\sqrt{1 - k^2 \sin^2 \theta}} = \\ = & \int_0^x \frac{dt}{\sqrt{1 - t^2}\sqrt{1 - k^2 t^2}} ; \quad (43a) \end{aligned}$$

$$\begin{aligned} E(k, \beta) = & \int_0^\beta \sqrt{1 - k^2 \sin^2 \theta} d\theta = \\ = & \int_0^x \frac{\sqrt{1 - k^2 t^2}}{\sqrt{1 - t^2}} dt ; \quad (43b) \end{aligned}$$

$$x = \sin \beta ; \quad t = \sin \theta ; \quad (43c)$$

for further details refer to specialized textbooks (e.g. Spiegel 1968, Chap. 4, §§34.1-4).

Using Eqs. (23b), (23c) and (39)-(42), the PP macrogases equation of state is obtained from the particularization of Eq. (26) to the case of interest for the domain, $y \geq 1$. The extension to the domain, $0 \leq y \leq 1$, can be carried out following the procedure outlined in Subsection 2.4.

In the absence of truncation radius, the density drops to zero as the radius goes to infinity, $\Xi \rightarrow +\infty$, $\eta \rightarrow +\infty$, and Eqs. (38)-(42) reduce to:

$$\lim_{\Xi_u \rightarrow +\infty} F_u(\xi_u) = \frac{2^{7/2}}{3} \frac{1}{(1 + \xi_u^2)^{3/2}} ; \quad (44)$$

$$\lim_{\Xi_u \rightarrow +\infty} (\nu_u)_{\text{mas}} = 2^{5/2} ; \quad (45)$$

$$\lim_{\Xi_u \rightarrow +\infty} (\nu_u)_{\text{sel}} = \frac{3\pi}{2} ; \quad (46)$$

$$\lim_{\eta \rightarrow +\infty} w^{(\text{int})}(\eta) = -\frac{128}{3} (y^\dagger)^2 \frac{[(y^\dagger)^2 + 7]E(k, \pi/2)}{3[(y^\dagger)^2 - 1]^3} - \frac{[5(y^\dagger)^2 + 3]F(k, \pi/2)}{3[(y^\dagger)^2 - 1]^3} ;$$

$$k = \sqrt{1 - (y^\dagger)^2} ; \quad y^\dagger \neq 1 ; \quad (47a)$$

$$\lim_{\eta \rightarrow +\infty} w^{(\text{int})}(\eta) = -\frac{4\pi}{3} ; \quad y^\dagger = 1 ; \quad (47b)$$

$$\lim_{\eta \rightarrow +\infty} w^{(\text{ext})}(\eta) = -\frac{128}{3} y^\dagger \frac{[3(y^\dagger)^2 + 5]F(k, \pi/2)}{3[(y^\dagger)^2 - 1]^3} - \frac{[7(y^\dagger)^2 + 1]E(k, \pi/2)}{3[(y^\dagger)^2 - 1]^3} ;$$

$$k = \sqrt{1 - 1/(y^\dagger)^2} ; \quad y^\dagger \neq 1 ; \quad (48a)$$

$$\lim_{\eta \rightarrow +\infty} w^{(\text{ext})}(\eta) = -\frac{4\pi}{3} ; \quad y^\dagger = 1 ; \quad (48b)$$

where, in particular, the related expression of the tidal energy coincides with its counterpart calculated in an earlier attempt (Valentinuzzi 2006, Chap. 4, §4.1). Using Eqs. (23b), (23c) and (45)-(48), the PP macrogases equation of state in the special situation under discussion is obtained from the particularization of Eq. (26) to the case of interest, for the domain, $y \geq 0$.

If, in addition, $y = y^\dagger = 1$, $\Xi_j = \Xi_i$, the combination of Eqs. (26) and (45)-(48) yields Eq. (36).

3.3. HH macrogases

The related density profiles (Hernquist 1990) imply $(\alpha, \beta, \gamma) = (1, 4, 1)$, and Eq. (27) reduces to:

$$f_u(\xi_u) = \frac{8}{\xi_u(1 + \xi_u)^3} ;$$

$$0 \leq \xi_u \leq \Xi_u ; \quad u = i, j ; \quad (49)$$

which has been proved to be consistent with nonnegative distribution functions, in the parameter range of interest (Ciotti 1996).

The particularization of Eqs. (17a), (18b), (20c), (24a), and (24b) to the case of interest yields:

$$F_u(\xi_u) = \frac{8}{(1 + \xi_u)^2} - \frac{8}{(1 + \Xi_u)^2} ; \quad (50)$$

$$(\nu_u)_{\text{mas}} = \frac{12\Xi_u^2}{(1 + \Xi_u)^2} ; \quad (51)$$

$$(\nu_u)_{\text{sel}} = \frac{12\Xi_u^3(4 + \Xi_u)}{(1 + \Xi_u)^4} ; \quad (52)$$

$$w^{(\text{int})}(\eta) = -128y^\dagger \left\{ \frac{1}{2} \frac{1}{(y^\dagger - 1)^4} \left[-\frac{(y^\dagger - 1)^2 y^\dagger \eta}{(y^\dagger \eta + 1)^2} + \frac{2(y^\dagger - 1)\eta}{1 + \eta} + \frac{(y^\dagger - 1)(y^\dagger + 3)y^\dagger \eta}{y^\dagger \eta + 1} + 2(2y^\dagger + 1) \ln \frac{\eta + 1}{y^\dagger \eta + 1} \right] - \frac{1}{2} \frac{1}{(1 + \Xi_j)^2} \frac{1}{(y^\dagger)^2} \left[1 - \frac{2y^\dagger \eta + 1}{(y^\dagger \eta + 1)^2} \right] \right\} ;$$

$$y^\dagger \neq 1 ; \quad (53a)$$

$$w^{(\text{int})}(\eta) = -128 \left\{ \frac{1}{12} \left[-\frac{4\eta + 1}{(\eta + 1)^4} + 1 \right] - \frac{1}{2} \frac{1}{(1 + \Xi_j)^2} \frac{\eta^2}{(\eta + 1)^2} \right\} ;$$

$$y^\dagger = 1 ; \quad (53b)$$

$$w^{(\text{ext})}(\eta) = -128 \left\{ -\frac{1}{2} \frac{1}{(y^\dagger - 1)^4} \left[\frac{(y^\dagger - 1)^2 \eta}{(\eta + 1)^2} + \frac{2(y^\dagger)^2 (y^\dagger - 1)\eta}{1 + y^\dagger \eta} + \frac{(y^\dagger - 1)(3y^\dagger + 1)\eta}{\eta + 1} - 2y^\dagger (y^\dagger + 2) \ln \frac{y^\dagger \eta + 1}{\eta + 1} \right] - \frac{1}{2} \frac{1}{(1 + \Xi_i)^2} \frac{\eta^2}{(\eta + 1)^2} \right\} ;$$

$$y^\dagger \neq 1 ; \quad (54a)$$

$$w^{(\text{ext})}(\eta) = 128 \left\{ \frac{1}{12} \left[\frac{4\eta + 1}{(\eta + 1)^4} - 1 \right] + \frac{1}{2} \frac{1}{(1 + \Xi_i)^2} \frac{\eta^2}{(\eta + 1)^2} \right\} ;$$

$$y^\dagger = 1 ; \quad (54b)$$

using Eqs. (23b), (23c) and (51)-(54), the HH macrogases equation of state is obtained from the particularization of Eq. (26) to the case of interest for the domain, $y \geq 1$. The extension to the domain,

$0 \leq y \leq 1$, can be carried out following the procedure outlined in Subsection 2.4.

In the absence of truncation radius, the density drops to zero when the radius tends to infinity, $\Xi \rightarrow +\infty$, $\eta \rightarrow +\infty$, and Eqs. (50)-(54) reduce to:

$$\lim_{\Xi_u \rightarrow +\infty} F_u(\xi_u) = \frac{8}{(1 + \xi_u)^2} ; \quad (55)$$

$$\lim_{\Xi_u \rightarrow +\infty} (\nu_u)_{\text{mas}} = 12 ; \quad (56)$$

$$\lim_{\Xi_u \rightarrow +\infty} (\nu_u)_{\text{sel}} = 12 ; \quad (57)$$

$$\begin{aligned} \lim_{\eta \rightarrow +\infty} w^{(\text{int})}(\eta) = & -\frac{64y^\dagger}{(y^\dagger - 1)^4} [-2(2y^\dagger + 1) \ln y^\dagger + \\ & + (y^\dagger - 1)(y^\dagger + 5)] ; \\ & y^\dagger \neq 1 ; \end{aligned} \quad (58a)$$

$$\lim_{\eta \rightarrow +\infty} w^{(\text{int})}(\eta) = -\frac{32}{3} ; \quad y^\dagger = 1 ; \quad (58b)$$

$$\begin{aligned} \lim_{\eta \rightarrow +\infty} w^{(\text{ext})}(\eta) = & -\frac{64}{(y^\dagger - 1)^4} [2y^\dagger(y^\dagger + 2) \ln y^\dagger - \\ & - (y^\dagger - 1)(5y^\dagger + 1)] ; \\ & y^\dagger \neq 1 ; \end{aligned} \quad (59a)$$

$$\lim_{\eta \rightarrow +\infty} w^{(\text{ext})}(\eta) = -\frac{32}{3} ; \quad y^\dagger = 1 ; \quad (59b)$$

where, in particular, the corresponding expression for the tidal energy coincides with its counterpart calculated in an earlier attempt (Valentinuzzi 2006, Chap. 4, §4.2.1). Using Eqs. (23b), (23c) and (56)-(59), the HH macrogases equation of state, in the special situation under discussion, is obtained from the particularization of Eq. (26) to the case of interest for the domain, $y \geq 0$. If, in particular, $y = y^\dagger = 1$, $\Xi_j = \Xi_i$, the combination of Eqs. (26) and (56)-(59) yields Eq. (36).

3.4. HP macrogases

The inner density profile (Hernquist 1990) implies $(\alpha, \beta, \gamma) = (1, 4, 1)$, which is defined by Eq. (49), and related functions and parameters by Eqs. (50)-(52) or (55)-(57) in the special case of no truncation radius.

The outer density profile (Schuster 1883, Plummer 1911) implies $(\alpha, \beta, \gamma) = (2, 5, 0)$, which is defined by Eq. (37), and related functions and parameters by Eqs. (38)-(40) or (44)-(46) in the special case of no truncation radius.

With respect to the tidal potential-energy terms, the particularization of Eqs. (24a) and (24b) to the case of interest yields:

$$\begin{aligned} w^{(\text{int})}(\eta) = & -\frac{128\sqrt{2}}{3} y^\dagger \left[\Phi_1^{(\text{int})}(\eta) + \Phi_2^{(\text{int})}(\eta) - \right. \\ & \left. - \frac{1}{2} \frac{\eta^2}{(1 + \Xi_j)^{3/2}} \right] ; \end{aligned} \quad (60a)$$

$$\begin{aligned} \Phi_1^{(\text{int})}(\eta) = & \frac{(y^\dagger)^4 - 12(y^\dagger)^2 + 2}{2[(y^\dagger)^2 + 1]^3} + \\ & + \frac{P^{(\text{int})}(\eta)}{2[(y^\dagger)^2 + 1]^3 (y^\dagger \eta + 1)^2 (\eta^2 + 1)^{1/2}} ; \end{aligned} \quad (60b)$$

$$\begin{aligned} \Phi_2^{(\text{int})}(\eta) = & -\frac{3y^\dagger [3(y^\dagger)^2 - 2]}{2[(y^\dagger)^2 + 1]^{7/2}} \cdot \\ & \cdot \ln \frac{[y^\dagger - \eta + \sqrt{(y^\dagger)^2 + 1} \sqrt{\eta^2 + 1}]}{(y^\dagger \eta + 1) [y^\dagger + \sqrt{(y^\dagger)^2 + 1}]} ; \end{aligned} \quad (60c)$$

$$\begin{aligned} P^{(\text{int})}(\eta) = & -2(y^\dagger)^5 \eta (2\eta^2 + 1) + (y^\dagger)^4 (\eta^2 - 1) + \\ & + (y^\dagger)^3 \eta (11\eta^2 + 15) + \\ & + 4(y^\dagger)^2 (4\eta^2 + 3) + 2y^\dagger \eta - 2 ; \end{aligned} \quad (60d)$$

$$\begin{aligned} w^{(\text{ext})}(\eta) = & -64\sqrt{2} \left[\Phi_1^{(\text{ext})}(\eta) + \Phi_2^{(\text{ext})}(\eta) - \right. \\ & \left. - \frac{1}{3} \frac{1}{(1 + \Xi_i)^2} \frac{\eta^3}{(1 + \eta^2)^{3/2}} \right] ; \end{aligned} \quad (61a)$$

$$\begin{aligned} \Phi_1^{(\text{ext})}(\eta) = & \frac{11(y^\dagger)^3 - 4y^\dagger}{3[(y^\dagger)^2 + 1]^3} + \\ & + \frac{P^{(\text{ext})}(\eta)}{3[(y^\dagger)^2 + 1]^3 (y^\dagger \eta + 1) (\eta^2 + 1)^{3/2}} ; \end{aligned} \quad (61b)$$

$$\begin{aligned} \Phi_2^{(\text{ext})}(\eta) = & \frac{(y^\dagger)^2 [2(y^\dagger)^2 - 3]}{[(y^\dagger)^2 + 1]^{7/2}} \cdot \\ & \cdot \ln \frac{[y^\dagger - \eta + \sqrt{(y^\dagger)^2 + 1} \sqrt{\eta^2 + 1}]}{(y^\dagger \eta + 1) [y^\dagger + \sqrt{(y^\dagger)^2 + 1}]} ; \end{aligned} \quad (61c)$$

$$\begin{aligned} P^{(\text{ext})}(\eta) = & (y^\dagger)^5 \eta^2 (2\eta^2 + 3) - (y^\dagger)^4 \eta (4\eta^2 + 5) - \\ & - (y^\dagger)^3 (12\eta^4 + 21\eta^2 + 11) - (y^\dagger)^2 \eta (3\eta^2 + 5) + \\ & + y^\dagger (\eta^4 + 6\eta^2 + 4) + \eta^3 ; \end{aligned} \quad (61d)$$

using Eqs. (23b), (23c), (39), (40), (51), and (52), the HP macrogases equation of state is obtained from the particularization of Eq. (26) to the case of interest for the domain, $y \geq 1$.

In absence of truncation radius, the density drops to zero when the radius tends to infinity, $\Xi \rightarrow +\infty$, $\eta \rightarrow +\infty$, and Eqs. (38)-(40), (50)-(52), reduce to (44)-(46), (55)-(57), respectively, and Eqs. (60)-(61) reduce to:

$$\begin{aligned} \lim_{\eta \rightarrow +\infty} w^{(\text{int})}(\eta) = & -\frac{64\sqrt{2}y^\dagger}{3[(y^\dagger)^2 + 1]^3} \cdot \\ & \cdot \left\{ [(y^\dagger)^4 - 4(y^\dagger)^3 - 12(y^\dagger)^2 + 11y^\dagger + 2] - \right. \\ & \left. - \frac{3y^\dagger [3(y^\dagger)^2 - 2]}{\sqrt{(y^\dagger)^2 + 1}} \ln \frac{\sqrt{(y^\dagger)^2 + 1} - 1}{y^\dagger [y^\dagger + \sqrt{(y^\dagger)^2 + 1}]} \right\} ; \\ & y^\dagger \neq 1 ; \end{aligned} \quad (62a)$$

$$\lim_{\eta \rightarrow +\infty} w^{(\text{int})}(\eta) = \frac{8}{3} \left[2\sqrt{2} + 3 \ln \frac{\sqrt{2}-1}{\sqrt{2}+1} \right] ;$$

$$y^\dagger = 1 ; \quad (62b)$$

$$\lim_{\eta \rightarrow +\infty} w^{(\text{ext})}(\eta) = -\frac{64\sqrt{2}}{3[(y^\dagger)^2 + 1]^3} \cdot \left\{ [2(y^\dagger)^4 + 11(y^\dagger)^3 - 12(y^\dagger)^2 - 4y^\dagger + 1] - \frac{3(y^\dagger)^2[-2(y^\dagger)^2 + 3]}{\sqrt{(y^\dagger)^2 + 1}} \ln \frac{\sqrt{(y^\dagger)^2 + 1} - 1}{y^\dagger [y^\dagger + \sqrt{(y^\dagger)^2 + 1}]} \right\}$$

$$y^\dagger \neq 1 ; \quad (63a)$$

$$\lim_{\eta \rightarrow +\infty} w^{(\text{ext})}(\eta) = \frac{8}{3} \left[2\sqrt{2} + 3 \ln \frac{\sqrt{2}-1}{\sqrt{2}+1} \right] ;$$

$$y^\dagger = 1 ; \quad (63b)$$

where, in particular, the related expression of the tidal energy coincides with its counterpart calculated in an earlier attempt (Valentinuzzi 2006, Chap. 4, §4.2.2). Using Eqs. (23b), (23c) and (45), (46), (56), (57), (60), (61), the HP macrogases equation of state in the special situation under discussion, is obtained from the particularization of Eq. (26) to the case of interest, for the domain, $y \geq 0$.

3.5. HN macrogases

The inner density profile (Hernquist 1990) implies $(\alpha, \beta, \gamma) = (1, 4, 1)$, which is defined by Eq. (49), and related functions and parameters by Eqs. (50)-(52) or (55)-(57) in the special case of no truncation radius.

The outer density profile (Navarro et al. 1995, 1996, 1997) implies $(\alpha, \beta, \gamma) = (1, 3, 1)$, and Eq. (27) reduces to:

$$f_j(\xi_j) = \frac{4}{\xi_j(1 + \xi_j)^2} ; \quad 0 \leq \xi_j \leq \Xi_j ; \quad (64)$$

which, together with its H counterpart expressed by Eq. (49), has been proved to be consistent with nonnegative distribution functions, in the parameter range of interest (Lowenstein and White 1999).

The particularization of Eqs. (17a), (18b), and (20c) to the case of interest yields:

$$F_j(\xi_j) = \frac{8}{1 + \xi_j} - \frac{8}{1 + \Xi_j} ; \quad (65)$$

$$(\nu_j)_{\text{mas}} = 12 \left[\ln(1 + \Xi_j) - \frac{\Xi_j}{1 + \Xi_j} \right] ; \quad (66)$$

$$(\nu_j)_{\text{sel}} = 36 \frac{\Xi_j(2 + \Xi_j) - 2(1 + \Xi_j) \ln(1 + \Xi_j)}{(1 + \Xi_j)^2} ; \quad (67)$$

with respect to the tidal potential-energy terms, the particularization of Eqs. (24a) and (24b) to the case of interest yields:

$$w^{(\text{int})}(\eta) = -\frac{64y^\dagger}{(y^\dagger - 1)^3} \left[-\frac{(y^\dagger - 1)^2}{y^\dagger} \cdot \frac{y^\dagger \eta (y^\dagger \eta + 2)}{(y^\dagger \eta + 1)^2} + \frac{2y^\dagger \eta (y^\dagger - 1)}{y^\dagger \eta + 1} + 2 \ln \frac{\eta + 1}{y^\dagger \eta + 1} - \frac{(y^\dagger - 1)^3}{1 + \Xi_j} \frac{\eta^2}{(y^\dagger \eta + 1)^2} \right] ;$$

$$y^\dagger \neq 1 ; \quad (68a)$$

$$w^{(\text{int})}(\eta) = -\frac{64\eta^2}{(\eta + 1)^2} \left[\frac{\eta + 3}{3(\eta + 1)} - \frac{1}{1 + \Xi_j} \right] ;$$

$$y^\dagger = 1 ; \quad (68b)$$

$$w^{(\text{ext})}(\eta) = -\frac{64}{(y^\dagger - 1)^2} \left\{ -\frac{\eta}{\eta + 1} - \frac{y^\dagger \eta}{y^\dagger \eta + 1} - \frac{y^\dagger + 1}{y^\dagger - 1} \ln \frac{\eta + 1}{y^\dagger \eta + 1} - \frac{(y^\dagger - 1)^2}{(1 + \Xi_i)^2} \left[-\frac{\eta}{\eta + 1} + \ln(\eta + 1) \right] \right\} ;$$

$$y^\dagger \neq 1 ; \quad (69a)$$

$$w^{(\text{ext})}(\eta) = -64 \left\{ \frac{1}{6} \frac{\eta^2(\eta + 3)}{(\eta + 1)^3} - \frac{1}{(1 + \Xi_i)^2} \cdot \left[-\frac{\eta}{\eta + 1} + \ln(\eta + 1) \right] \right\} ;$$

$$y^\dagger = 1 ; \quad (69b)$$

using Eqs. (23b), (23c), (51), (52), (66), and (67), the HN macrogases equation of state is obtained from the particularization of Eq. (26) to the case of interest for the domain, $y \geq 1$.

In the absence of truncation radius, the density drops to zero when the radius tends to infinity, $\Xi \rightarrow +\infty$, $\eta \rightarrow +\infty$, and Eqs. (50)-(52), reduce to (55)-(57), respectively, whereas Eqs. (65)-(69) reduce to:

$$\lim_{\Xi_j \rightarrow +\infty} F_j(\xi_j) = \frac{8}{1 + \xi_j} ; \quad (70)$$

$$\lim_{\Xi_j \rightarrow +\infty} (\nu_j)_{\text{mas}} = +\infty ; \quad (71)$$

$$\lim_{\Xi_j \rightarrow +\infty} (\nu_j)_{\text{sel}} = 36 ; \quad (72)$$

$$\lim_{\eta \rightarrow +\infty} w^{(\text{int})}(\eta) = -\frac{64}{(y^\dagger - 1)^3} \cdot [(y^\dagger)^2 - 1 - 2y^\dagger \ln y^\dagger] ;$$

$$y^\dagger \neq 1 ; \quad (73a)$$

$$\lim_{\eta \rightarrow +\infty} w^{(\text{int})}(\eta) = -\frac{64}{3} ; \quad y^\dagger = 1 ; \quad (73b)$$

$$\lim_{\eta \rightarrow +\infty} w^{(\text{ext})}(\eta) = -\frac{64}{(y^\dagger - 1)^2} \cdot \left[-2 + \frac{y^\dagger + 1}{y^\dagger - 1} \ln y^\dagger \right] ; \quad y^\dagger \neq 1 ; \quad (74a)$$

$$\lim_{\eta \rightarrow +\infty} w^{(\text{ext})}(\eta) = -\frac{32}{3} ; \quad y^\dagger = 1 ; \quad (74b)$$

where the self potential-energy profile factor remains finite, although the mass profile factor undergoes a logarithmic divergence. Using Eqs. (23b), (23c) and (72)-(74), the HN macrogases equation of state (where M_j^\dagger and m^\dagger appear instead of M_j and m) in the situation under consideration, is obtained from the particularization of Eq. (26) to the case of interest, for the domain, $y \geq 0$.

4. RESULTS

The macrogases equation of state, Eq. (26), is shown in the following figures for a number of cases analysed in Section 3. In particular, owing to Eqs. (34) and (35), the UU macrogases equation of state is independent of the scaled truncation radii, (Ξ_i, Ξ_j) .

The macrogases equation of state in absence of truncation radius, is plotted in Fig. 1 for cases (from top left in clockwise sense) UU, PP, HH, HP, where $\Xi_j = \Xi_i$ and (from bottom to top in each panel) $m = 1, 2, \dots, 6$, for cases UU, PP, HP, and $m = 10, 20, \dots, 60$, for case HH. Shallower density profiles (UU, PP) show the occurrence of two extremum points: one minimum on the left and one maximum on the right, for any values of the fractional mass, m . Steeper density profiles (HP, HH) still exhibit extremum points, but none below a threshold, where the critical isofractional mass curve shows a single horizontal inflexion point.

As already noticed in an earlier attempt (CS90), the same trend is shown by van der Waals' (1873) isothermal curves and, in fact, the van der Waals' equation of state looks similar to the macrogases equation of state, Eq. (26), where three variables also appear. Thick curves represent the locus of minimum (left branch) and maximum (right branch) points. The critical isofractional mass curve, when it appears, is also thickened.

A main feature is that, above the critical isofractional mass curve, for any selected value of m , a range in fractional virial potential energy, ϕ , exists, $\phi_{\min} < \phi < \phi_{\max}$, where three different con-

figurations i.e. different fractional truncation radius, y , correspond to the same value of ϕ . By analogy with van der Waals' isothermal curves, one could argue the existence of a bell-shaped region in the $Oy\phi$ plane, within which the extremum points are located, and where a phase transition occurs. Further investigation is needed on this point, but it lies outside the aim of the current paper.

The macrogases equation of state in presence of truncation radius is plotted in Figs. 2 and 3, respectively, for different choices of the fractional truncation radii, (Ξ_i, Ξ_j) , represented on each panel where (from bottom to top) $m = 10, 20, \dots, 60$, and approximate values of the parameters related to the critical point i.e. the horizontal inflexion point on the critical isofractional mass curve (marked by a St. Andrew's cross), are listed in Table 1.

Table 1. Approximate values of parameters related to the critical point i.e. the horizontal inflexion point on the critical isofractional mass curve, for the density profiles under investigation. Dashes instead of numbers mean the absence of the critical curve in the corresponding case. Numbers in brackets denote the values of scaled truncation radii, (Ξ_i, Ξ_j) . In the absence of truncation radius, $\Xi \rightarrow +\infty$, the case considered is $\Xi_j/\Xi_i \rightarrow 1$, which implies $y^\dagger = y$. For homogeneous configurations (case UU) the isofractional mass curves are independent of (Ξ_i, Ξ_j) .

case	(Ξ_i, Ξ_j)	m^\dagger	m	y^\dagger	y	φ
HN	(05-05)	—	—	—	—	—
	(05-10)	04.41	09.45	1.04	2.08	09.16
	(05-20)	05.14	15.49	1.14	4.56	13.44
	(10-05)	03.17	03.68	0.88	0.44	03.90
	(10-10)	06.36	11.46	1.38	1.38	11.48
	(10-20)	07.24	18.33	1.50	3.00	16.47
	(20-05)	04.99	05.27	1.18	0.29	05.75
	(20-10)	08.10	13.30	1.62	0.81	13.74
	(20-20)	09.10	20.99	1.75	1.75	19.48
	HH	(05-05)	07.10	07.10	2.32	2.32
(05-10)		07.72	09.19	2.43	4.86	08.17
(05-20)		07.90	10.32	2.45	9.80	08.62
(10-05)		11.15	09.37	3.18	1.59	09.44
(10-10)		11.88	11.88	3.30	3.30	11.03
(10-20)		12.10	13.28	3.33	6.66	11.57
(20-05)		15.00	11.50	3.77	0.94	12.04
(20-10)		15.83	14.42	3.88	1.94	13.94
(20-20)		16.08	16.08	3.92	3.92	14.60
(∞ - ∞)		20.22	20.22	4.27	4.27	18.15
HP	(∞ - ∞)	04.59	04.59	2.05	2.05	06.03
PP	(∞ - ∞)	—	—	—	—	—
UU	(Ξ_i, Ξ_j)	—	—	—	—	—

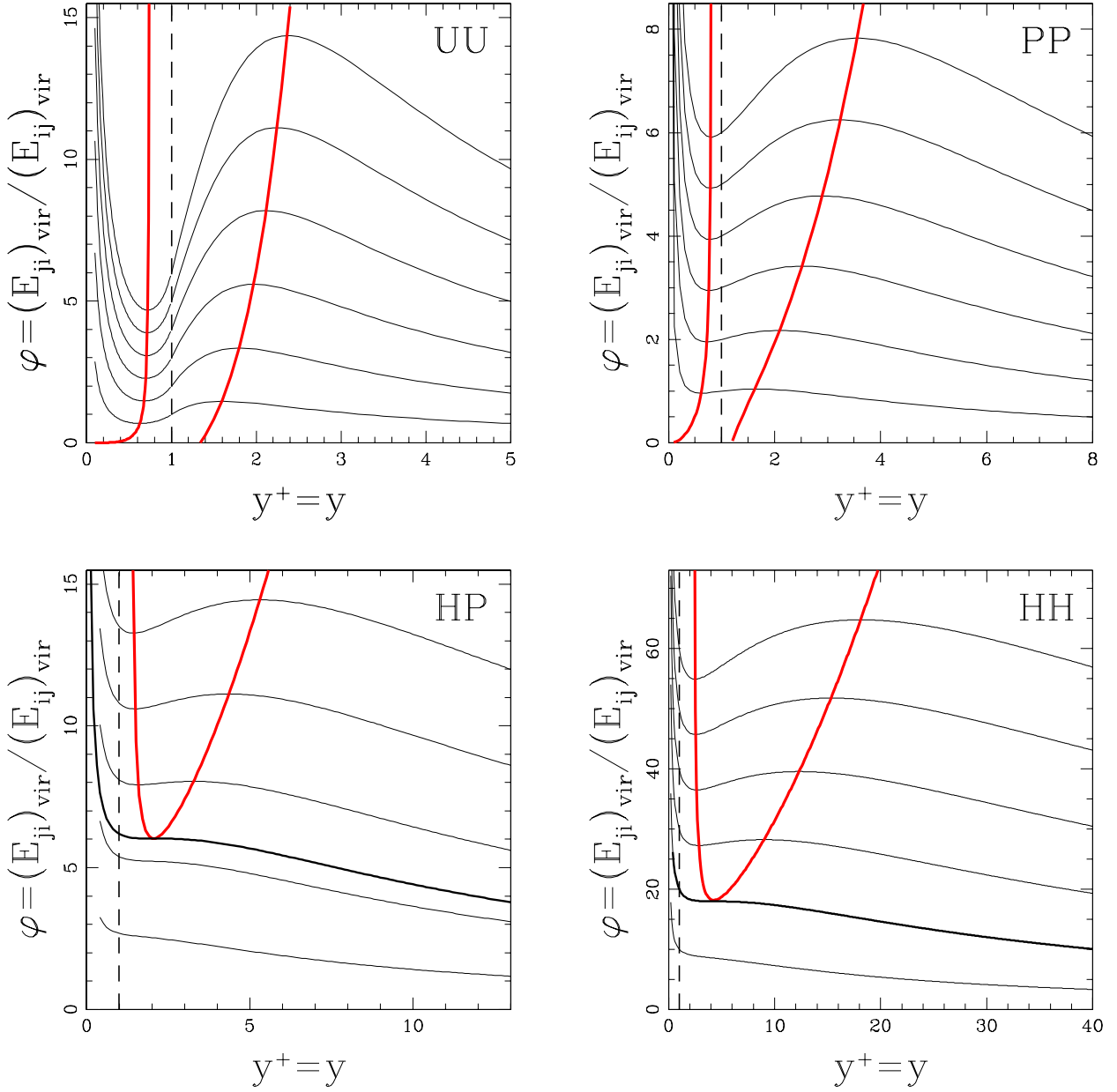


Fig. 1. Isofractional mass curves related to (from top left in clockwise sense) UU, PP, HH, HP, macrogases for $\Xi \rightarrow +\infty$, $\Xi_j/\Xi_i \rightarrow 1$. Thick curves represent the locus of minimum (left branch) and maximum (right branch) points. The critical curve is also thickened, and the horizontal inflexion point, or critical point, is defined (when present) as the tangent point with respect to the locus of the extremum points. The value of the fractional mass is $m = \phi(1, m)$ and can be read on the intersection between the selected curve and the dashed vertical line, $y^\dagger = y = 1$, provided the density profile of the inner and the outer subsystem belong to the same family (UU, PP, HH). All the curves diverge at $y \rightarrow 0$ and converge to 0 at $y \rightarrow +\infty$. For UU macrogases, the extremum points of the $m = 0$ isofractional mass curve occur at $y = 0$ and $y = 3/\sqrt{5}$, respectively, and the locus of the minimum points has a vertical asymptote, $y = \sqrt{5}/3$. For PP macrogases, the extremum points of the $m = 0$ isofractional mass curve occur at $y = 0$ and $y \approx 1.20$, respectively, and the locus of the minimum points has a vertical asymptote, $y \approx 0.84$.

It can be seen that the occurrence of the truncation radius makes little change to the trend of the isofractional mass curves. In general, decreasing the outer scaled truncation radius, Ξ_j , yields more pronounced extremum points and vice versa. Much smaller changes, in the same sense, are produced by decreasing the inner scaled truncation radius, Ξ_i . This is why, in the cases under discussion, the mass of the outer subsystem is dominant with respect to the mass of the inner subsystem, $m \gg 1$. The critical isofractional mass curve does not appear for earlier truncated HN density profiles, $(\Xi_i, \Xi_j) = (5, 5)$,

which are shallower than their latter truncated counterparts.

Reduced truncation radii, $\Xi = R/r^\dagger$, may be conceived as concentrations of the related matter distribution (e.g. Navarro et al. 1997, CM03, Caimmi et al. 2005) and the selected range, $5 \leq \Xi \leq 20$, is consistent with the results of dark matter (hereafter quoted as DM) halo numerical simulations (e.g. Bullock et al. 2001) and elliptical galaxy (hereafter quoted as EG) observations (e.g. Lowenstein and White 1999).

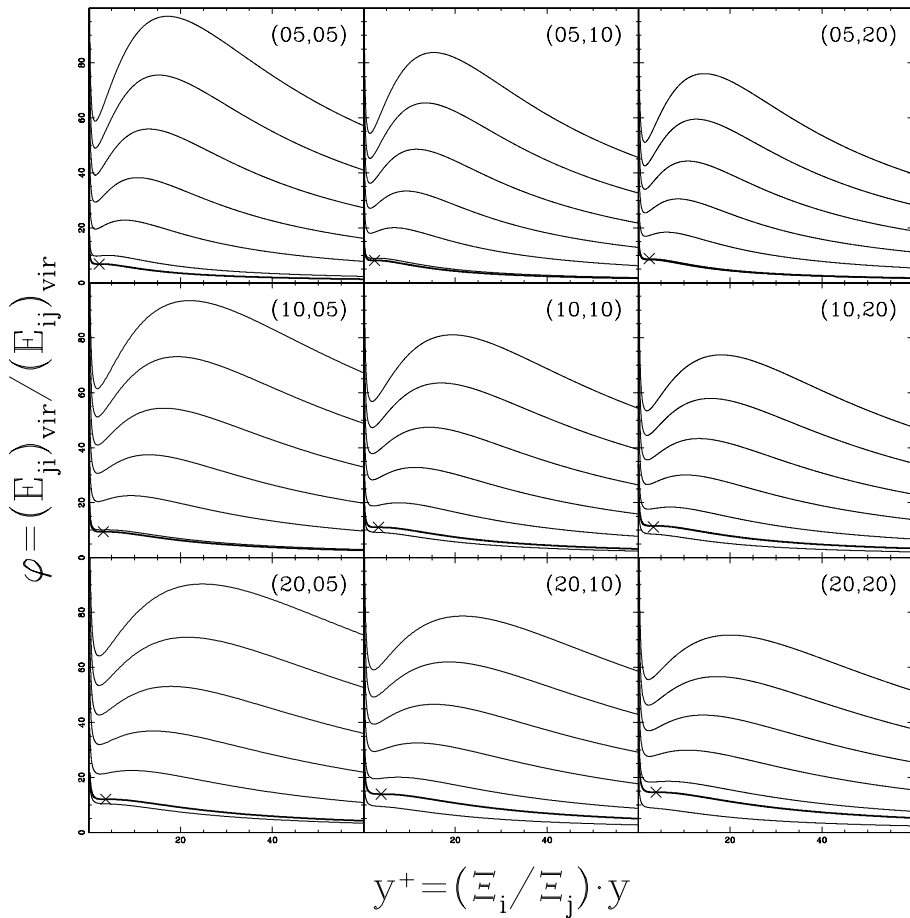


Fig. 2. Isofractional mass curves pertaining to HH macrogases, for different choices of scaled truncation radii, (Ξ_i, Ξ_j) , indicated on each panel, where (from bottom to top) $m = 10, 20, \dots, 60$. The critical isofractional mass curve, with the horizontal inflexion point or critical point, marked by a St. Andrew's cross, is thickened on each panel. All the curves diverge at $y \rightarrow 0$ and converge to 0 at $y \rightarrow +\infty$.

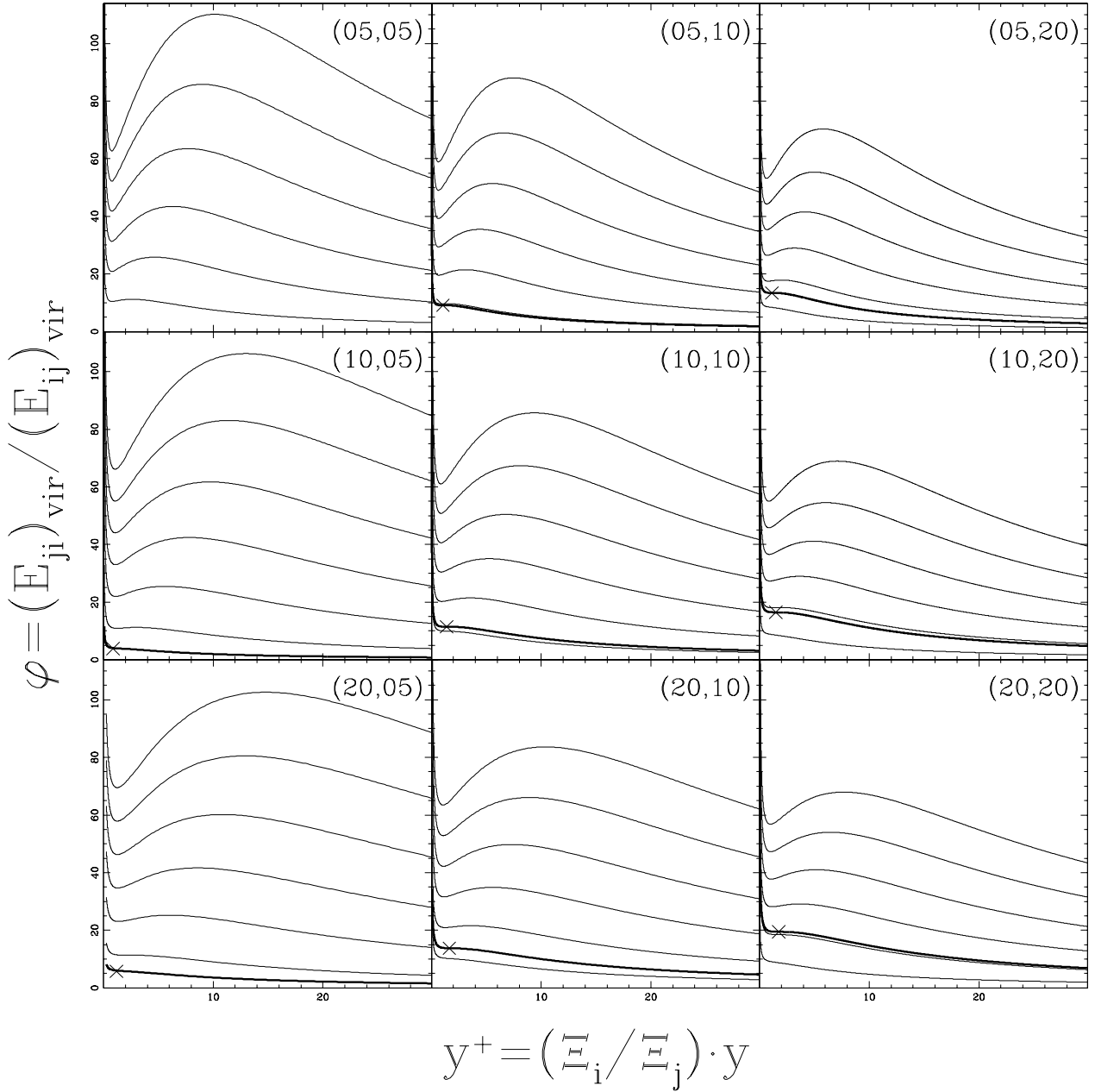


Fig. 3. Isofractional mass curves pertaining to HN macrogases, for different choices of scaled truncation radii, (Ξ_i, Ξ_j) , indicated on each panel, where (from bottom to top) $m = 10, 20, \dots, 60$. The critical isofractional mass curve, with the horizontal inflexion point or critical point, marked by a St. Andrew's cross, is thickened on each panel. All the curves diverge at $y \rightarrow 0$ and converge to 0 at $y \rightarrow +\infty$.

5. APPLICATION TO ELLIPTICAL GALAXIES AND THEIR HOSTING HALOES

According to current cosmological scenarios (e.g. Mota and van de Bruck 2004, Percival 2005, Horellou and Berge 2005, Maor and Lahav 2005, Nunes and Mota 2006), density perturbations at recombination epoch ($z \approx 1100$) initially expand with the universe, turn around, collapse, and finally virialize (at least in their inner and denser regions).

Virialized density perturbations, such as typical elliptical galaxies (EGs) and clusters of galaxies, may be idealized, to a first extent, as two homeoidally striated, similar and similarly placed, density profiles. In the following, attention shall be focused on EGs.

5.1. General considerations and main assumptions

A recent investigation performed on an optically complete sample of 42 EGs, for which X-ray gas temperatures and central stellar velocity dispersions were determined (Davis and White 1996), has shown evidence that, in general, EGs contain substantial amounts of DM (Loewenstein and White 1999). Accordingly, more than about 20% and 39%-85% of the total mass within one and six optical radii, respectively, is in form of (non baryonic) DM, depending on the stellar density profile and observed value of X-ray gas temperature and central stellar velocity dispersion. The comparison between the velocity dispersion distributions for DM and stars, assuming isotropic orbits, shows that the DM is dynamically "hotter" than the stars, by a factor 1.4-2 (Loewenstein and White 1999).

The above investigation cannot be considered as conclusive in favour of the existence of DM haloes hosting EGs. In fact, it has been pointed out that the attenuation (in particular, the scattering) by dust grains has the same effect on the stellar kinematics as a DM halo (Baes and Dejonghe 2001). According to a recent attempt, no strong evidence for DM haloes within 1-3 optical radii has been found in a restricted sample of 4 early-type EGs, using dynamical modelling (Samurovic and Danziger 1995). Beyond 1-3 optical radii, the X-ray methodology shows the need of DM wherever an X-ray halo is detected (Samurovic and Danziger 1995). A similar trend is exhibited by an additional early-type EG (Samurovic and Danziger, 1996). In any case, current cosmological scenarios (Λ CDM, QCDM) predict DM haloes hosting EGs, as well as spiral galaxies, for which there are lots of empirical evidence (e.g. flat rotation curves well outside optical radii). For this reason, EGs are also assumed to be embedded within DM haloes.

An analysis on the evolution of the physical properties of cosmological baryons at low redshifts ($z \lesssim 5$) has recently been performed (Valageas et

al. 2002), which (i) yields robust model-independent results that agree with numerical simulations; (ii) recovers the fraction of matter within different phases and the spatial clustering computed by numerical simulations; (iii) predicts a soft X-ray background due to the "warm" intergalactic medium component, that is consistent with observations. The related baryon fraction in the present universe is found to be 7% in hot gas, 24% in the warm intergalactic medium, 38% in the cool intergalactic medium, 9% within star-like objects and, as a still unobserved component, 22% of dark baryons associated with collapsed structures, with a relative uncertainty no larger than 30% on these figures. Then the amount of still undetected baryons is about one fifth of the total, one fourth of the observed baryons (intergalactic medium, stellar components, and hot gas), and at least twice the stellar-like component.

According to recent investigations, HH (e.g. Ciotti 1996) or HN (e.g. Loewenstein and White 1999) models provide viable representations for the inner, baryonic, and the outer, nonbaryonic subsystem, respectively. The above mentioned mass distributions were found to be self-consistent, in the parameter range of interest, with regard to the non negativity of the distribution function (e.g. Ciotti 1996, Loewenstein and White 1999) by use of a theorem stated in an earlier attempt (Ciotti and Pellegrini 1992).

If undetected baryons in EGs are present as hot gas, the gaseous subsystem is expected to be less concentrated than the stellar one, as in the Coma cluster of galaxies (e.g. Briel et al. 1992). If undetected baryons in EGs are present as unseen stars, the undetected subsystem is expected to be as concentrated as the stellar one. Either assumption is necessary in dealing with two-component systems. The real situation lies between the limiting cases mentioned.

The typical velocity dispersion components, deduced by use of the virial theorem (hereafter referred to, in general, as the virial velocity dispersions) are global quantities, related to the virial potential energy of the subsystem as a whole, and so, by construction, independent of the specific orbital distribution of the particles. This important property, however, is also a weakness of the virial theorem, in dealing with velocity dispersion components measured in the central region of a galaxy. In fact, it is well known that the related values can significantly differ for structurally identical subsystems (and so characterized by identical virial velocity dispersion components), due to different orbital structures (e.g. de Zeeuw and Franx 1991). When using central velocity dispersion components, an approach based on Jeans equations (even though still questionable) is to be preferred (e.g. Ciotti et al. 1996, Ciotti and Lanzoni 1997, Loewenstein and White 1999). On the other hand, a comparison between the results obtained by use of either of the above mentioned methods, may provide additional support to both of them and/or useful indications on the nature of the problem under investigation.

Strictly speaking, the central velocity dispersions (along the line of sight) in EGs, as deduced from observations, should be scaled to the virial velocity dispersions. Both observational evidence (e.g. Gerhard et al. 2001) and theoretical arguments (e.g. Nipoti et al. 2002) point towards the existence of dynamical homology in EGs. In particular, a linear relation is found between a local parameter, averaged central velocity dispersion, and a global parameter, inferred maximum circular velocity, $\sigma_{0.1} = (2/3)(v_c)_{max}$ (Gerhard et al. 2001). Accordingly, the central velocity dispersion components are expected to be proportional to the virial velocity dispersion components. Then it could be assumed that the related proportionality factor is of the order of unity.

In fact, typical peculiar velocity component distributions within EGs show a maximum which is rapidly attained in the central region (at about 1 kpc), and a slow decrease occurs moving outwards (no more than about 13% the maximum at about 10 kpc), at least in the case of isotropic orbits; for further details see related attempts (e.g. Loewenstein and White 1999). Accordingly, both the central and the virial velocity dispersion components are expected to be of comparable order, slightly less than the maximum of the peculiar velocity component distribution (e.g. Cappellari et al. 2006). On the other hand, most EGs are moderately radially anisotropic (e.g. Gerhard et al. 2001), and the related variation in central velocity dispersion (an increase for increasing σ_i^2 and vice versa) is also expected to be moderate.

5.2. Input parameters, specific assumptions, and results

The main assumptions of the current model are (i) homeoidally striated density profiles and (ii) similar and similarly placed boundaries. Aspherical, heterogeneous, self-gravitating fluids in dynamical or hydrostatic equilibrium exhibit isopycnic surfaces different from ellipsoids (e.g. Chandrasekhar 1933, Chandrasekhar and Lebovitz 1962, Vandervoort and Welty 1981, Lai et al. 1993), and the above assumption (i) is due to reasons of simplicity.

Axisymmetric configurations with nonsimilar boundaries have been investigated in the special case of homogeneous density profiles i.e. UU macrogases, where the shape of one component is kept fixed and an additional variable, the axis ratio of the other component, together with an additional relation, the angular momentum conservation of the other component, must be considered (CS90). A main feature is that the isofractional mass curves on the $(Oy\phi)$ plane cannot converge to 0 at $y \rightarrow +\infty$, as the ending point occurs when the inner subsystem attains a flat configuration. For further details refer to the parent paper (CS90). Being the calculations for heterogeneous density profiles much more complicated, the above assumption (ii) is also due to reasons of simplicity. It can be expected that the effect due to nonsimilar boundaries is maximum for homoge-

neous density profiles, and decreases as the profile is steeper, to be null for mass points surrounded by a massless atmosphere (Roche ellipsoids). Then the results found for homogeneous density profiles (CS90) make a valid reference for inhomogeneous density profiles. In conclusion, the above assumptions (i) and (ii) are related to a viable model which can be used for specific applications to large-scale celestial objects, in particular EGs.

Given a typical EG, a natural question (in the light of the model under discussion) arises about its position on the $(Oy\phi)$ plane for assigned density profiles and specified input parameters. Towards this aim, the following main assumptions are made: (a) the stellar and the DM distributions are described by homeoidally striated, similar and similarly placed, HH or HN density profiles, respectively; (b) undetected baryons trace either DM haloes or EGs; and (c) the virial theorem holds for each subsystem within the tidal potential of the other one.

According to the above assumptions, a typical EG embedded in a DM halo is idealized as two homeoidally striated, similar and similarly placed matter distributions, where the star and non baryonic subsystem are described by HH or HN density profiles, respectively.

For assigned density profiles, the macrogases equation of state, Eq. (26), depends on two independent variables: the fractional truncation radius, $y = R_j/R_i$, and the fractional mass, $m = M_j/M_i$, or their scaling counterparts, $y^\dagger = r_j^\dagger/r_i^\dagger$ and $m^\dagger = M_j^\dagger/M_i^\dagger$. To represent celestial objects in the $(Oy\phi)$ plane, two additional equations are requested. Having in mind an application to EGs and their hosting haloes, denoted in the following by the indices i and j , respectively, for $y \geq 1$, an additional relation between the stellar projected velocity dispersion, $(\sigma_i)_{R_e/8}$, averaged over the aperture used for spectroscopic observations ($r = R_e/8$), and the fractional scaling radius, y^\dagger , may be deduced from the virial theorem related to the star subsystem, Eq. (8b), by solving the appropriate Jeans equations, following an earlier approach (Ciotti et al. 1996). The result may be written as:

$$(\sigma_i)_{R_e/8}^2 = \frac{GM_i}{r_i^\dagger} \psi_i(y^\dagger, m^\dagger) ; \quad (75)$$

where ψ_i is a function calculated by a numerical algorithm.

Use of Eq. (75) implies further restrictions, as its validity is limited to (i) spherically-symmetric matter distributions; (ii) isotropic peculiar velocity distributions; (iii) infinite truncation radii; (iv) HH density profiles. Concerning points (i)-(iii) mentioned above, acceptable approximations may safely be expected. On the other hand, HH density profiles provide a viable description to EGs embedded within DM haloes (e.g. Ciotti 1996).

At this stage, an additional relation is needed. The mere existence of a fundamental plane (Djorgovski and Davis 1987, Dressler et al. 1987) indi-

cates that structural properties in EGs span a narrow range, suggesting that some self-regulating mechanism must be at work during formation and evolution. In particular, projected light profiles from EGs exhibit large degree of homogeneity and may well be fitted by the de Vaucouleurs $r^{1/4}$ law. Accordingly, a narrow range may safely be expected also for EG fractional mass and the assumption, $m = \text{const}$, appears to be a viable approximation. The last, together with Eqs. (26) and (75), makes a system of three equations in the three unknowns, ϕ , y , m , via Eqs. (21), for HH density profiles. Then the position of EGs and their hosting haloes on a selected isofractional mass curve in the $(Oy\phi)$ plane, can be determined.

The sample used ($N = 16$) is extracted from a larger sample ($N = 25$) of EGs and lenticular galaxies investigated within the SAURON project (Cappellari et al. 2006, Table 1 therein), for which the parameters of interest i.e. masses, projected central velocity dispersions, and effective radii, can be derived from the data listed in Table 2.

More specifically, with regard to the inner (stellar) subsystem, projected central velocity dispersions are deduced from the luminosity-

weighted second moment of the line-of-sight velocity distribution within the effective radius, σ_e , as $(\sigma_i)_{R_e/8} = 8^{0.066}\sigma_e$; masses are deduced from luminosities and mass-luminosity ratios (in I -band), as $M_i/M_{10} = (L/L_\odot)[(M_i/L)/(10^{10}m_\odot/L_\odot)]$; $L/L_\odot = \exp_{10}\{-0.4[I_T - (\hat{m} - \hat{M}) - 4.11]\}$; scaling radii are calculated from effective radii (in arcsec) and distances, by use of a profile factor, equal to 1.81, related to the case under discussion (Hernquist 1990), as $r_i^\dagger/\text{kpc} = (R_e/\text{kpc})/1.81$; $R_e/\text{kpc} = [(R_e/\text{arcsec})(d/\text{Mpc})]/206.265$; $d/\text{Mpc} = \exp_{10}[(\hat{m} - \hat{M})/5 - 5]$. For further details refer to the parent paper (Cappellari et al. 2006).

The substitution of the selected value of the fractional mass, m , into Eq. (75), allows the value of the fractional scaling radius, y^\dagger , for each sample object. Finally, the substitution of (y^\dagger, m) values into Eq. (26), particularized to HH density profiles via Eqs. (56)-(59), allows the value of the fractional virial potential energy, ϕ , and the position of each sample object on a selected isofractional mass curve in the $(Oy\phi)$ plane, can be determined.

Table 2. Data related to a subsample ($N = 16$) extracted from a sample ($N = 25$) of EGs and lenticular galaxies investigated within the SAURON project (Cappellari et al. 2006), and deduced values of the parameters of interest. Column caption: (1) NGC number; (2) effective (half-light) radius, R_e , measured in the I -band; (3) total observed I -band galaxy magnitude; (4) mass-luminosity ratio (including DM) deduced from the best fitting three-integral Schwarzschild model, computed at a fiduciary inclination; (5) mass-luminosity ratio of the stellar population; (6) galaxy distance modulus (hats avoid confusion with the fractional mass, m , and the total mass, M); (7) galaxy mass, calculated as $M_i/M_{10} = (L/L_\odot)[(M_i/L)/(10^{10}m_\odot/L_\odot)]$; $L/L_\odot = \exp_{10}\{-0.4[I_T - (\hat{m} - \hat{M}) - 4.11]\}$; (8) galaxy central velocity dispersion, deduced from the luminosity-weighted second moment of the line-of-sight velocity distribution within the effective radius, σ_e , as $(\sigma_i)_{R_e/8} = 8^{0.066}\sigma_e$; (9) galaxy scaling radius, calculated as $r_i^\dagger/\text{kpc} = (R_e/\text{kpc})/1.81$; $R_e/\text{kpc} = [(R_e/\text{arcsec})(d/\text{Mpc})]/206.265$; $d/\text{Mpc} = \exp_{10}[(\hat{m} - \hat{M})/5 - 5]$. The factor, 1.81, is related to an assumed Hernquist profile for the inner subsystem (Hernquist 1990). The factor, 206.265, is related to the choice of measure units. For further details refer to the parent paper (Cappellari et al. 2006).

NGC	R_e (arcsec)	I_T (mag)	M/L (I -band)	M_i/L (I -band)	$(\hat{m} - \hat{M})$ (mag)	M_i (M_{10})	$(\sigma_i)_{R_e/8}$ (km s^{-1})	r_i^\dagger (kpc)
(1)	(2)	(3)	(4)	(5)	(6)	(7)	(8)	(9)
0821	039.0	09.47	3.08	2.60	31.85	10.26	216.80	2.45
2974	024.0	09.43	4.52	2.34	31.60	07.61	267.28	1.34
3377	038.0	08.98	2.22	1.75	30.19	02.35	158.30	1.11
3379	042.0	08.03	3.36	3.08	30.06	08.80	230.57	1.16
3608	041.0	09.40	3.71	2.57	31.74	09.77	204.19	2.45
4278	032.0	08.83	5.24	3.05	30.97	09.64	264.98	1.34
4374	071.0	07.69	4.36	3.08	31.26	36.35	318.90	3.40
4458	027.0	10.68	2.28	2.27	31.12	01.50	097.50	1.21
4473	027.0	08.94	2.91	2.88	30.92	07.86	220.24	1.10
4486	105.0	07.23	6.10	3.33	30.97	45.97	341.84	4.40
4552	032.0	08.54	4.74	3.35	30.87	12.62	289.07	1.28
4621	046.0	08.41	3.03	3.12	31.25	18.80	242.04	2.19
4660	011.0	09.96	3.63	2.96	30.48	02.11	212.21	0.37
5813	052.0	09.12	4.81	2.97	32.48	28.89	263.83	4.36
5845	004.6	11.10	3.72	2.96	32.01	03.02	274.16	0.31
5846	081.0	08.41	5.30	3.33	31.92	37.19	273.01	5.25

The results are plotted for various choices of scaled truncation radii, (Ξ_i, Ξ_j) , and different choices of fractional masses, m , in Fig. 4.

Isofractional mass curves, $m = 10$ (top panels), and $m = 20$ (bottom panels), are labelled by the

selected choices of scaled truncation radii, (Ξ_i, Ξ_j) , indicated near the corresponding curves, and the sample objects are represented as dots. Curves lie above and below the critical curve for $m = 10$, while all curves lie above the critical curve for $m = 20$, with respect to the cases considered.

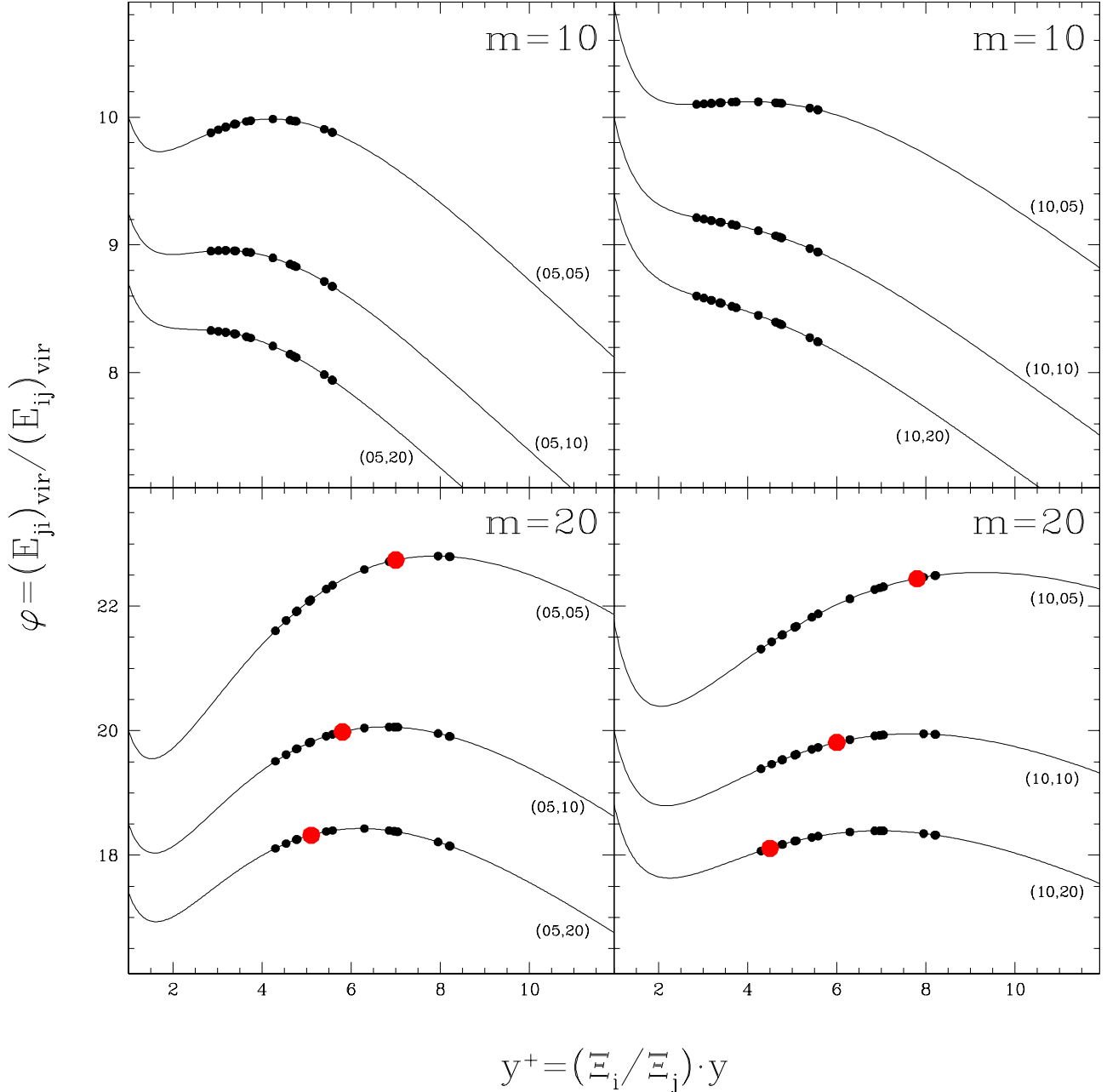


Fig. 4. Isofractional mass curves, $m = 10$ (top panels), and $m = 20$ (bottom panels), pertaining to HH macrogases, for different choices of scaled truncation radii, (Ξ_i, Ξ_j) , as indicated near the corresponding curves, and corresponding positions of $N = 16$ EGs (dots), listed in Table 2. Different cases correspond to vertical shifts of the sample objects. Larger dots represent configurations where the virial potential energy of the inner subsystem attains the maximum value with respect to a frozen outer subsystem.

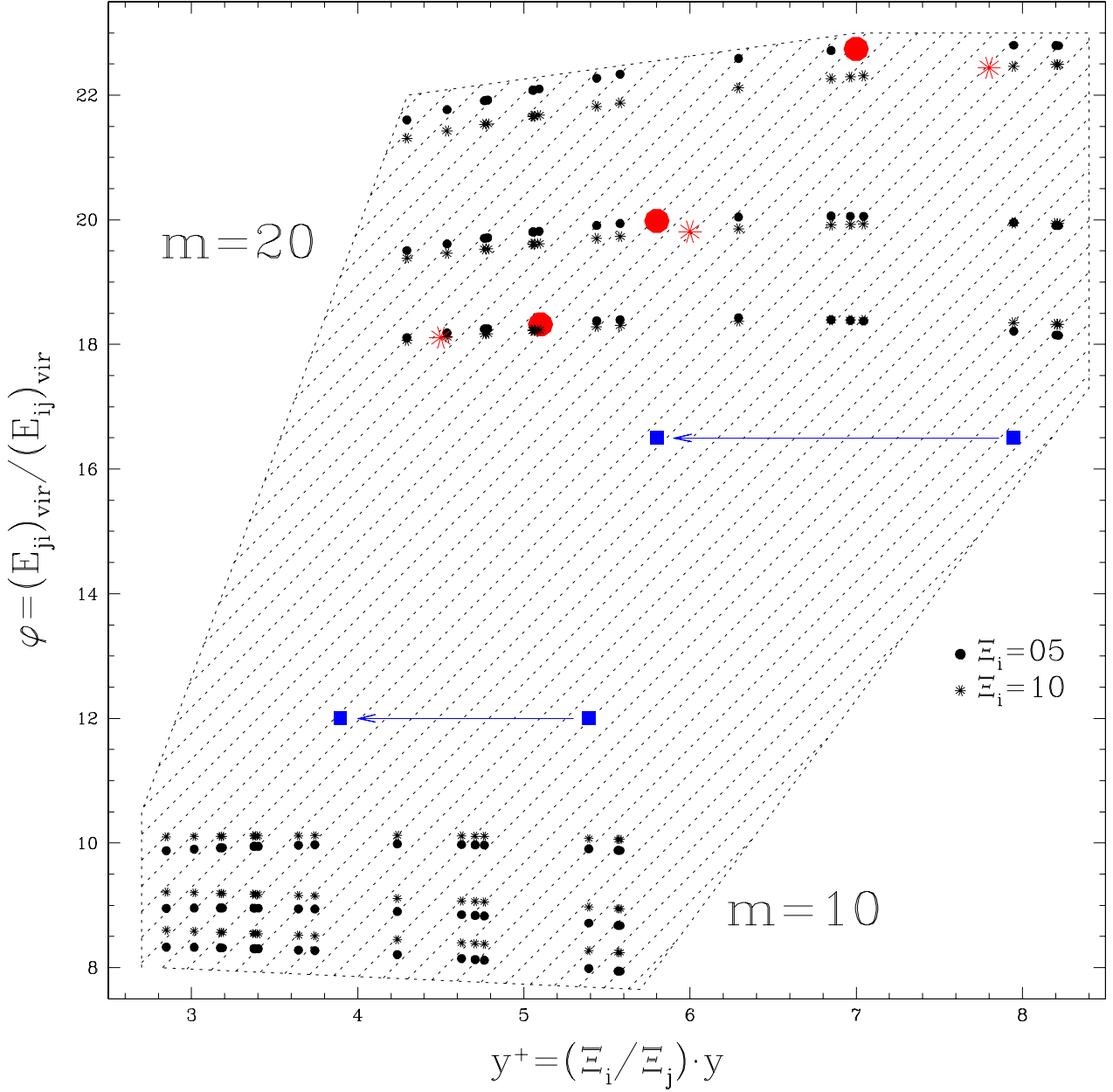


Fig. 5. The parameter space of the cases plotted in Fig. 4, roughly outlined by the shaded region. Dots and asterisks correspond to inner scaled truncation radii, $\Xi_i = 5$ and 10 , respectively. For fixed fractional mass, m , the corresponding outer scaled truncation radii read $\Xi_j = 5, 10, 20$, from top to bottom. Small and large symbols represent sample objects and configurations where the virial potential energy of the inner subsystem attains the maximum value with respect to a frozen outer subsystem, respectively. No such configuration exists in the cases considered, for fractional masses, $m \lesssim 20$. The related parameter space is restricted to a region close to the angle defined by the locus of large dots and asterisks, respectively. The intersection between the above mentioned loci occurs for outer scaled truncation radii, Ξ_j , slightly larger than 10 . The change of position for NCG 3379, due to a change in effective radius, from $R_e = 42.0$ to $R_e = 54.8$, is indicated by squares, regardless of the vertical scale.

The above description is due to the reasons of simplicity, but the model does not necessarily imply that sample objects must be located on the same isofractional mass curve and/or correspond to the same scaled truncation radii. What is relevant is the position of EGs on the $(Oy\phi)$ plane, which implies the following assumptions: (i) there are in the universe 16 EGs with intrinsic values of the parameters equal to their counterparts listed in Table 2 for sample objects, and (ii) related star distributions are well described by H density profiles.

In fact, observational uncertainties on the quantities of interest (Cappellari et al. 2006) contribute to large errors in the fractional scaling radius, y^\dagger . As an example, a single galaxy, NGC 3379, and a single parameter, the effective radius, shall be considered. In the case under discussion, $R_e = (42.0 \mp 7.1)$ arcsec (Cappellari et al. 2006), but different estimates exist, such as (54.8 ∓ 3.5) arcsec (Capaccioli et al. 1990) which is consistent with the above result within $2\sigma_{R_e}$. Using the latter value, the fractional scaled radius, y^\dagger , passes from 5.74 to 4.08 for the fractional mass $m = 10$, and from 8.45 to 6.07 for $m = 20$.

Different values of parameters, m , Ξ_i , Ξ_j , make sample objects locate on different isofractional mass curves, as shown in Fig. 4, where y depends on m but is independent of Ξ_i and Ξ_j . Fiduciary values of the above mentioned parameters, say $10 \leq m \leq 20$, $5 \leq \Xi_u \leq 20$, $u = i, j$, define a region on the $(Oy\phi)$ plane, approximately as: $2.5 < y^\dagger < 6.0$, $7 < \phi < 11$, $m = 10$; $4 < y^\dagger < 9$, $17 < \phi < 23$, $m = 20$; where sample objects are positioned, as shown in Fig. 5.

Dots and asterisks correspond to inner scaled truncation radii, $\Xi_i = 5$ and 10, respectively. Small and large symbols represent sample objects and configurations where the virial potential energy of the inner subsystem attains the maximum value with respect to a frozen outer subsystem, respectively. No such configuration exists in the cases considered, for fractional masses, $m \lesssim 20$. The related parameter space is restricted to a region close to the angle defined by the locus of large dots and asterisks, respectively. The intersection between the above mentioned loci occurs for outer scaled truncation radii, Ξ_j , slightly larger than 10. The change of position for NCG 3379, due to a change in effective radius, from $R_e = 42.0$ to $R_e = 54.8$, is indicated by squares, regardless of the vertical scale.

In the special situation where the outer subsystem remains frozen and the inner one is free to contract or to expand, with unchanged mass and density profile, the virial potential energy of the inner subsystem may attain maximum (Secco 2000, 2001, 2005, Marmo and Secco 2003). For HH density profiles, lower fractional masses ($m = 10$) yield no extremum point, while the opposite holds for larger fractional masses ($m = 20$). The special configurations related to the maximum virial potential energy of the inner subsystem, when the outer subsystem remains frozen (hereafter quoted as "the maximum configuration"), are represented as large dots

in Fig. 4 (bottom panels) and large dots and asterisks in Fig. 5.

The maximum configuration appears to have little relevance in the light of the current model for a number of reasons. Firstly, it occurs for fractional masses above a threshold. Secondly, the loci of maximum configurations on the $(Oy\phi)$ plane show no correlation with the parameter space of the model related to sample objects. More precisely, the loci of maximum configurations are narrower and extend from bottom left to top right, while sample objects lie on a broader and less inclined band, as shown in Fig. 5.

The position of the maximum configuration on the isofractional mass curves $m = 20$ depends on the concentration of the outer subsystem, while the position of sample objects can only be vertically shifted, as the fractional scaling radius, y^\dagger , is independent of the concentration, via Eq. (75). In this view, it is difficult to conceive maximum configurations as ending points of any evolutionary track on the $(Oy\phi)$ plane, even if observational uncertainties are high.

EG position on the $(Oy\phi)$ plane, in particular along an isofractional mass curve ($m = \text{const}$), represents the end point of evolutionary tracks on the above mentioned plane. The pertaining configurations may be thought of as virialized to a good extent, in that sample objects listed in Table 2 show no sign of ungoing merger and star formation burst. The coincidence of ending points with maximum configurations would imply, for fixed (m, Ξ_i, Ξ_j) : (i) a single ending point for all sample objects i.e. homologous evolution, and (ii) m above the threshold for the occurrence of maximum configurations, which does not necessarily happen, as shown in Fig. 4. On the contrary, the evolution of EGs appears to be non homologous, in the sense that different ending points take place along the selected isofractional mass curves defined by the HH macrogases equation of state.

Owing to Eqs. (9b) and (12b), the total energy of the virialized system reads:

$$E = \frac{1}{2}[(E_{ij})_{\text{vir}} + (E_{ji})_{\text{vir}}] = -(E_i)_{\text{kin}} - (E_j)_{\text{kin}} ; \quad (76)$$

and the combination of Eqs. (12b), (25), and (76) yields:

$$E = \frac{1}{2}(1+\phi)(E_{ij})_{\text{vir}} = -(1+\phi)(E_i)_{\text{kin}}; \phi = \frac{(E_j)_{\text{kin}}}{(E_i)_{\text{kin}}}; \quad (77)$$

where the kinetic energy of the inner subsystem, $(E_i)_{\text{kin}}$, may be deduced from observations, and the related total energy, E , may be read on the vertical axis of Fig. 4. Within the range, $\phi_{\text{min}} \leq \phi \leq \phi_{\text{max}}$, three configurations exist with same virial potential (or kinetic) energy ratio, ϕ , and fractional mass, m , but different fractional truncation radius, y .

The restriction to constant fractional mass also in time, makes evolutionary tracks on the $(Oy\phi)$ plane locate on the related isofractional mass curve, ($m = \text{const}$), where displacements from the left to the right (increasing y values) are due to energy dis-

sipation, and displacements from the right to the left (decreasing y values) are due to energy acquisition. In the former alternative, changes in ϕ and $(E_{ij})_{\text{vir}}$ must act to yield a decreasing E (increasing in absolute value), the larger energy change being related to the larger y change. For further details refer to Appendix 2. In this view, the maximum configuration corresponds to a special energy change, $(\Delta E)_{\text{max}}$, and to a special y change, $(\Delta y)_{\text{max}}$. But there is no apparent reason for any special amount of energy to be dissipated, starting from the beginning of evolution, to attain the maximum configuration. A similar result holds in the latter alternative. In fact, it can be seen in Fig. 4 that the sample objects show no connection with the maximum configuration. Then the maximum configuration, which implies a frozen outer subsystem, has no special relevance in the light of the current model. For an analysis of different theories on the maximum configuration, refer to a specific study (Valentinuzzi 2006, Chaps. 5-5).

The above results hold if the baryonic subsystem is mainly in form of stars. Let us take into consideration a different scenario, where a less concentrated gaseous subsystem than the stellar one is also present, as in the Coma cluster of galaxies (e.g. Briel et al. 1992), and assume the same mass distribution as in the non baryonic matter to preserve use of two-component models (Caimmi 2003). Accordingly, a typical EG is idealized as formed by an inner subsystem made of stars and an outer subsystem made of gas and non baryonic matter. As the amount, of baryonic and non baryonic matter have to remain unchanged, the inner and the outer subsystem are less and more massive, respectively, than in absence of undetected baryons. Again, it is assumed that the related mass distributions are represented by HH density profiles. Then a similar procedure may be followed, keeping in mind that the fractional mass m is the ratio of nonbaryonic + extragalactic gas mass to star mass. For further details refer to an earlier attempt (CM03).

6. CONCLUSION

The two-component systems were regarded as (two-component) macrogases, and the related equation of state was formulated using the virial theorem for subsystems (Limber 1959, Brosche et al. 1983, Caimmi et al. 1984, Caimmi and Secco 1992), under the restriction of (i) homeoidally striated ellipsoids (Roberts 1962) and (ii) similar and similarly placed boundaries.

Explicit calculations were carried out for a useful reference case and a few cases of astrophysical interest, both in presence and in absence of truncation radius. More specifically, the following cases have been dealt with: IJ= UU, PP, HH, HP, HN, where I and J denote the inner and the outer density profile, respectively, and the other captions relate to the following density profiles: U ($\rho = \text{const}$), P (Plummer 1911), H (Hernquist 1990), N (Navarro

et al. 1995, 1996, 1997). Shallower density profiles (UU, PP), have been found to yield an equation of state, $\phi = \phi(y, m)$, characterized by the appearance of two extremum points, one maximum and one minimum, as in an earlier attempt (CS90). Steeper density profiles (HH, HP, HN), were found to produce a similar equation of state where, in addition, a single horizontal inflexion point occurs in a critical isofractional mass curve, and isofractional mass curves pertaining to lower values, $m = M_j/M_i < m_{\text{crit}}$, show no extremum point. The similarity between isofractional mass curves and van der Waals' isothermal curves, has suggested the possibility that a phase transition could take place in a bell-shaped region of the $(Oy\phi)$ plane.

Further investigation was devoted to HH density profiles for which a numerical algorithm (Ciotti et al. 1996) was used to represent EGs and their hosting DM haloes along selected isofractional mass curves on the $(Oy\phi)$ plane, under the assumption that the related fractional mass has the same value in different systems. In the light of the model, the evolution of EGs was found to be not strictly homologous, in the sense that the end of evolutionary tracks on the $(Oy\phi)$ plane occur at different points along the related isofractional mass curve, instead of being close to a single point.

Acknowledgements – We are indebted to an anonymous referee for critical comments which improved an earlier version of the manuscript. Thanks are due to L. Secco for fruitful discussions. The analytical integrations needed in the current paper were helped substantially by use of the Mathematica package and visiting the internet site: "HTTP://INTEGRALS.WOLFRAM.COM/INDEX.CGI". This is why we are deeply grateful to the Wolfram staff, in particular to Daniel Lichtblau, and wish to acknowledge all the facilities encountered therein.

REFERENCES

- Baes, M., Dejonge, H.: 2001, *Astrophys. J.*, **563**, L19.
 Bett, P., Eke, V., Frenk, C. et al.: 2007, *Mon. Not. R. Astron. Soc.*, **376**, 215.
 Briel, U. G., Henry, J. P., Böhringer, H.: 1992, *Astron. Astrophys.*, **259**, L31.
 Binney, J., Tremaine, S.: 1987. *Galactic Dynamics*, Princeton University Press, Princeton.
 Brosche, P., Caimmi, R., Secco, L.: 1983, *Astron. Astrophys.*, **125**, 338.
 Bullock, J. S., Kolatt, T. S., Sigad, J. et al.: 2001, *Mon. Not. R. Astron. Soc.*, **321**, 559.
 Caimmi, R.: 1986, *Astron. Astrophys.*, **159**, 147.
 Caimmi, R.: 1992, *Astron. Nachr.*, **313**, 165.
 Caimmi, R.: 1993, *Astrophys. J.*, **419**, 615.
 Caimmi, R.: 1995, *Astrophys. J.*, **441**, 533.
 Caimmi, R.: 2003, *Astron. Nachr.*, **324**, 250.
 Caimmi, R.: 2006, *App. Math. Comp.*, **174**, 447.
 Caimmi, R.: 2007a, *Serb. Astron. J.*, **174**, 13.

- Caimmi, R.: 2007b, *New Astronomy*, **12**, 327.
- Caimmi, R.: Secco, L., Brosche, P.: 1984, *Astron. Astrophys.*, **139**, 411.
- Caimmi, R.: Secco, L.: 1990, *Astron. Astrophys.*, **237**, 336 (CS90).
- Caimmi, R.: Secco, L.: 1992, *Astrophys. J.*, **395**, 119.
- Caimmi, R., Secco, L.: 2003, *Astron. Nachr.*, **324**, 491.
- Caimmi, R., Marmo, C.: 2003, *New Astronomy*, **8**, 119 (CM03).
- Caimmi, R., Marmo, C.: 2004, *Serb. Astron. J.*, **169**, 11.
- Caimmi, R., Marmo, C., Valentinuzzi, T.: 2005, *Serb. Astron. J.*, **170**, 13.
- Capaccioli, M., Held, E. V., Lorenz, H. et al.: 1990, *Astron. J.*, **99**, 1813.
- Cappellari, M., Bacon, R., Bureau, M. et al.: 2006, *Mon. Not. R. Astron. Soc.*, **366**, 1126.
- Carlberg, R. G., Yee, H. K. C., Ellingson, E. et al.: 1996, *Astrophys. J.*, **462**, 32.
- Chandrasekhar, S.: 1933, *Mon. Not. R. Astron. Soc.*, **93**, 390.
- Chandrasekhar, S.: 1939, *An Introduction to the Study of the Stellar Structure*, University of Chicago Press.
- Chandrasekhar, S., Lebovitz, N.: 1962, *Astrophys. J.*, **136**, 1082.
- Chandrasekhar, S.: 1969, *Ellipsoidal Figures of Equilibrium*, Yale University Press, New Haven.
- Ciotti, L.: 1996, *Astrophys. J.*, **471**, 68.
- Ciotti, L.: 1999, *Astrophys. J.*, **520**, 574.
- Ciotti, L., Pellegrini, S.: 1992, *Mon. Not. R. Astron. Soc.*, **255**, 561.
- Ciotti, L., Lanzoni, B., Renzini, A.: 1996, *Mon. Not. R. Astron. Soc.*, **282**, 1.
- Ciotti, L., Lanzoni, B.: 1997, *Astron. Astrophys.*, **321**, 724.
- Clausius, R.: 1870, Sitz. Niedewheinischen Gesellschaft, Bonn, p. 114 [translated in *Phil. Mag.* 40, 112 (1870)].
- Davis, D. S., White, R. E., III: 1996, *Astrophys. J.*, **470**, L35.
- de Zeeuw, T., Franx, M.: 1991, *Annu. Rev. Astron. Astrophys.*, **29**, 239.
- Djorgovski, S. G., Davis, M.: 1987, *Astrophys. J.*, **313**, 59.
- Dressler, A., Lynden-Bell, D., Burstein, D. et al.: 1987, *Astrophys. J.*, **313**, 42.
- Emden, R.: 1907, *Gas Kugeln*, Leipzig.
- Gerhard, O., Kronawitter, A., Saglia, R. P., Bender, R.: 2001, *Astron. J.*, **121**, 1936.
- Girardi, M., Giuricin, G., Mardirossian, F. et al.: 1998, *Astrophys. J.*, **505**, 74.
- Hernquist, L.: 1990, *Astrophys. J.*, **356**, 359.
- Horedt, G. P.: 2004, *Polytropes*, ApSS Library, **506**, Kluwer Acad. Publ.
- Horellou, C., Berge, J.: 2005, *Mon. Not. R. Astron. Soc.*, **360**, 1393.
- Lai, D., Rasio, F. A., Shapiro, S. L.: 1993, *Astrophys. J. Suppl. Series*, **88**, 205.
- Landau, L., Lifchitz, E.: 1966, *Mecanique*, Mir, Moscow.
- Lane, J. H.: 1870, *Amer. J. Sci. Arts*, **50**, 57.
- Limber, D. N.: 1959, *Astrophys. J.*, **130**, 414.
- Lowenstein, M., White, R. E., III: 1999, *Astrophys. J.*, **518**, 50.
- MacMillan, W. D.: 1930, *The Theory of the Potential*, Dover Publications, New York, 1958.
- Marmo, C., Secco, L.: 2003, *New Astronomy*, **8**, 629.
- Maor, I., Lahav, O.: 2005, *Journal of Cosmology and Astroparticle Physics*, **7**, 3.
- Mota, D. F., van de Bruck, C.: 2004, *Astron. Astrophys.*, **421**, 71.
- Mouri, H., Taniguchi, Y.: 2003, *Astrophys. J.*, **585**, 250.
- Navarro, J. F., Frenk, C. S., White, S. D. M.: 1995, *Mon. Not. R. Astron. Soc.*, **275**, 720.
- Navarro, J. F., Frenk, C. S., White, S. D. M.: 1996, *Astrophys. J.*, **462**, 563.
- Navarro, J. F., Frenk, C. S., White, S. D. M.: 1997, *Astrophys. J.*, **490**, 493.
- Neutsch, W.: 1979, *Astron. Astrophys.*, **72**, 339.
- Nipoti, C., Londrillo, P., Ciotti, L.: 2002, *Mon. Not. R. Astron. Soc.*, **332**, 901.
- Nunes, N. J., Mota, D. F.: 2006, *Mon. Not. R. Astron. Soc.*, **368**, 751.
- Percival, W. J.: 2005, *Astron. Astrophys.*, **443**, 819.
- Plummer, H. C.: 1911, *Mon. Not. R. Astron. Soc.*, **71**, 460.
- Roberts, P. H.: 1962, *Astrophys. J.*, **136**, 1108.
- Samurovic, S., Danziger, I. J.: 2005, *Mon. Not. R. Astron. Soc.*, **363**, 769.
- Samurovic, S., Danziger, I. J.: 2006, *Astron. Astrophys.*, **458**, 79.
- Schuster, A.: 1883, *Brit. Ass. Rep.*, p. 428.
- Secco, L.: 2000, *New Astron.*, **5**, 403.
- Secco, L.: 2001, *New Astron.*, **6**, 339.
- Secco, L.: 2005, *New Astron.*, **10**, 349.
- Spiegel, M. R.: 1968, *Mathematical Handbook*, Schaum's Outline Series, McGraw-Hill, Inc., New York.
- The, L. S., White, S. D. M.: 1986, *Astron. J.*, **92**, 1248.
- Valageas, P., Schaeffer, R., Silk, J.: 2002, *Astron. Astrophys.*, **388**, 741.
- Valentinuzzi, T.: 2006, Unpublished PHD Thesis, Padua University.
- Vandervoort, P. O.: 1980, *Astrophys. J.*, **240**, 478.
- Vandervoort, P. O., Welty, D. E.: 1981, *Astrophys. J.*, **248**, 504.
- van der Waals, J. D.: 1873, *Over de Continuïteit van den Gas-en Vloeïstoftoestand*, (Doctoral Thesis).
- Zhao, H. S.: 1996, *Mon. Not. R. Astron. Soc.*, **278**, 488.

APPENDICES

**A1. Plummer density profiles and
 $n = 5$ polytropes**

The Lane-Emden equation reads (e.g. Lane 1870, Emden 1907, Chandrasekhar 1933, Horedt 2004, Chap. 4, §2.1):

$$\frac{1}{\xi_{\text{LE}}^2} \frac{d}{d\xi_{\text{LE}}} \left(\xi_{\text{LE}}^2 \frac{d\theta}{d\xi_{\text{LE}}} \right) = -\theta^n ; \quad (78a)$$

$$\theta(0) = 1 ; \quad \theta(\Xi_{\text{LE}}) = 0 ; \quad (78b)$$

$$\xi_{\text{LE}} = \frac{r}{\alpha_{\text{LE}}} ; \quad \Xi_{\text{LE}} = \frac{R}{\alpha_{\text{LE}}} ; \quad (78c)$$

$$\rho(r) = \lambda \theta^n(\xi_{\text{LE}}) ; \quad (78d)$$

where n is the polytropic index ($0 \leq n \leq 5$ and $0.5 < n \leq 5$ for realistic collisional and collisionless equilibrium configurations, respectively), α_{LE} is a scaling radius and λ is the central density.

In the special case $n = 5$, the integration of Eq. (78a) yields (Schuster 1883, see also Chandrasekhar 1939, Chap. IV, §4, Horedt 2004, Chap. 4, §2.3.3):

$$\theta(\xi_{\text{LE}}) = \left(1 + \frac{1}{3} \xi_{\text{LE}}^2 \right)^{-1/2} ; \quad (79a)$$

$$\Xi_{\text{LE}} \rightarrow +\infty ; \quad n = 5 ;$$

$$\frac{d\theta}{d\xi_{\text{LE}}} = -\frac{1}{3} \xi_{\text{LE}} \left(1 + \frac{1}{3} \xi_{\text{LE}}^2 \right)^{-3/2} ; \quad (79b)$$

$$-\xi_{\text{LE}}^2 \frac{d\theta}{d\xi_{\text{LE}}} = \sqrt{3} \left(\frac{\xi_{\text{LE}}}{\sqrt{3}} \right)^3 \left[1 + \left(\frac{\xi_{\text{LE}}}{\sqrt{3}} \right)^2 \right]^{-3/2} \quad (79c)$$

$$\lim_{\xi_{\text{LE}} \rightarrow +\infty} \left(-\xi_{\text{LE}}^2 \frac{d\theta}{d\xi_{\text{LE}}} \right) = \sqrt{3} ; \quad (79d)$$

and the general expression of a polytrope mass (e.g. Chandrasekhar 1939, Chap. IV, §4, Horedt 2004, Chap. 4, §2.6.3):

$$M = -4\pi \lambda \alpha_{\text{LE}}^3 \Xi_{\text{LE}}^2 \left(\frac{d\theta}{d\xi_{\text{LE}}} \right)_{\Xi_{\text{LE}}} ; \quad (80)$$

in the case of interest, using Eqs. (79), reduces to:

$$M = \sqrt{3} 4\pi \lambda \alpha_{\text{LE}}^3 ; \quad n = 5 ; \quad (81)$$

finally, the explicit expression of the density profile results from the combination of Eqs. (78d) and (79a), as:

$$\rho(r) = \lambda \left(1 + \frac{1}{3} \xi_{\text{LE}}^2 \right)^{-5/2} ; \quad n = 5 ; \quad (82)$$

and the following relation is derived from comparison with Eqs. (14a) and (27):

$$\rho^\dagger 2^\chi \xi^{-\gamma} (1 + \xi^\alpha)^{-\chi} = \lambda \left(1 + \frac{1}{3} \xi_{\text{LE}}^2 \right)^{-5/2} ; \quad (83)$$

which, in turn, implies the following:

$$\xi = \frac{\xi_{\text{LE}}}{\sqrt{3}} ; \quad \alpha_{\text{LE}} = \frac{\xi}{\xi_{\text{LE}}} r^\dagger = \frac{r^\dagger}{\sqrt{3}} ; \quad (84a)$$

$$\gamma = 0 ; \alpha = 2 ; \chi = \frac{5}{2} = \frac{\beta - \gamma}{\alpha} = \frac{\beta}{2} ; \beta = 5 ; \quad (84b)$$

$$\lambda = 2^{5/2} \rho^\dagger ; \quad (84c)$$

and the substitution of Eqs. (84a) and (84c) into (82) yields:

$$\rho(r) = \rho^\dagger f(\xi) ; \quad (85a)$$

$$f(\xi) = \frac{2^{5/2}}{(1 + \xi^2)^{5/2}} ; \quad (85b)$$

according to Eq. (37).

An equivalent formulation can be obtained by the combination of Eqs. (81) and (84). The result is:

$$\rho(r) = \frac{3M}{4\pi} \frac{(r^\dagger)^2}{[r^2 + (r^\dagger)^2]^{5/2}} ; \quad (86)$$

which is known as the Plummer (1911) density profile.

**A2. Quasi static contraction in
 presence of tidal potential**

The scalar virial equations, Eqs. (12b), for assigned density profiles i.e. fixed $\alpha_u, \beta_u, \gamma_u$, and Ξ_u , $u = i, j$, depend on four parameters e.g., masses and scaling radii, M_u and r_u^\dagger . The further assumption of spherical-symmetric matter distributions is only to simplify calculations. Let a specified amount of energy, $\Delta E < 0$, be instantaneously dissipated within the inner subsystem, as:

$$(E_i)_{\text{kin}} \rightarrow (E_i)_{\text{kin}} + \Delta E ; \quad (87)$$

and the system readjust to attain a new configuration in accordance with Eqs. (12b) where, in general, density profiles and scaling radii are changed, while masses and the outer subsystem truncation radius may be assumed fixed, or their variations specified. More specifically, density profiles are steepened by energy dissipation, and the system gets bounder i.e. a larger (in absolute value) binding energy is attained.

The further constraint of density profiles unaffected by energy dissipation, implies the following changes ($u = i, j$):

$$M_u \rightarrow M_u + \Delta M_u ; \quad \Delta M_u = 0 ; \quad (88a)$$

$$\Xi_u \rightarrow \Xi_u + \Delta \Xi_u ; \quad \Delta \Xi_u = 0 ; \quad (88b)$$

$$R_u \rightarrow R_u + \Delta R_u ; \quad \Delta R_j = 0 ; \quad (88c)$$

$$r_u^\dagger \rightarrow r_u^\dagger + \Delta r_u^\dagger ; \quad \Delta r_j^\dagger = 0 ; \quad (88d)$$

$$(E_u)_{\text{kin}} \rightarrow (E_u)_{\text{kin}} + \Delta E_u ; \quad (88e)$$

$$\Delta E_i + \Delta E_j = \Delta E ;$$

where the assumption that energy dissipation within the inner subsystem has no effect on (i) masses, M_u ; (ii) scaled truncation radii, Ξ_u ; density profiles, $(\alpha_u, \beta_u, \gamma_u)$; (iii) truncation radius of the outer subsystem, R_j ; implies a frozen outer subsystem. In general, the changes, $\Delta M_u = \zeta_m M_u$, $\Delta R_u = \zeta_u R_u$, and $\Delta r_u^\dagger = \zeta_u r_u^\dagger$, making m and Ξ_u conserved, should be specified. The application of the scalar virial theorem, Eqs. (12), to the subsystems before and after energy dissipation, yields:

$$U_{uv}(y^\dagger) + 2(E_u)_{\text{kin}} = 0 ; \quad (89a)$$

$$U_{uv}(y^\dagger + \Delta y^\dagger) + 2[(E_u)_{\text{kin}} + \Delta E_u] = 0 ; \quad (89b)$$

$$U_{uv} = (E_{uv})_{\text{vir}} ; \quad (89c)$$

where the fractional scaling radius, $y^\dagger = r_j^\dagger/r_i^\dagger$, has been chosen as variable.

The combination of Eqs. (89a) and (89b) yields:

$$\Delta(E_{uv})_{\text{vir}} + 2\Delta E_u = 0 ; \quad (90a)$$

$$\Delta(E_{uv})_{\text{vir}} = U_{uv}(y^\dagger + \Delta y^\dagger) - U_{uv}(y^\dagger) ; \quad (90b)$$

and the combination of Eqs. (90a), by use of (88e) produces:

$$\Delta(E_{ij})_{\text{vir}} + \Delta(E_{ji})_{\text{vir}} + 2\Delta E = 0 ; \quad (91)$$

which is a transcendental equation in Δy^\dagger provided the density profiles and the amount of dissipated energy, ΔE , are specified. In general, the changes, $\Delta M_u = \zeta_m M_u$, $\Delta R_u = \zeta_u R_u$, and $\Delta r_u^\dagger = \zeta_u r_u^\dagger$, which make m and Ξ_u conserved, should also be specified. Then the remaining parameters related to the relaxed system, due to energy dissipation, may be determined. In particular, $\Delta y^\dagger > 0$ is expected together with $m = \text{const}$ due to mass conservation in each subsystem or mass variation of the kind considered, $m = (M_j + \Delta M_j)/(M_i + \Delta M_i) = M_j/M_i$. Accordingly, the position of the system in the $(Oy\phi)$ plane moves from the left to the right along the related isofractional mass curve (see e.g., Fig. 4).

ФРАКЦИОНА ВИРИЈАЛНА ПОТЕНЦИЈАЛНА ЕНЕРГИЈА У ДВОКОМПОНЕНТНИМ СИСТЕМИМА

R. Caimmi and T. Valentiniuzzi

*Dipartimento di Astronomia, Università di Padova
Vicolo Osservatorio 2, I-35122 Padova, Italy*

E-mail: roberto.caimmi@unipd.it, tiziano.valentinuzzi@unipd.it

УДК 524.7–52–54 : 524.88

Оригинални научни рад

Разматрају се двокомпонентни системи као макрогасови и са тим у вези једначина стања се пише користећи виријалну теорему за подсистеме под претпоставком о постојању хомеоидално избразданих профила густина. Урађене су експлицитне рачунице за референтни случај и за неколико астрофизички интересантних случајева, и то са и без радијуса зарубљености. Показано је да плићи профили густине допуштају једначину стања, $\phi = \phi(y, m)$ коју карактерише (за задате вредности фракционе масе, $m = M_j/M_i$) постојање две екстремне тачке, минимума и максимума, како је показано у ранијем покушају. Стрмији профили густине дају сличну једначину стања, што имплицира да је специјална вредност m у вези са критичном кривом где се горе поменуће екстремне тачке своде на једну хоризонталну тачку кривине, а криве испод критичне не показују екстремне тачке. Сличност изофракционих кривих маса ван дер Валсовим изотермалним кривим сугерише могућност фазног

прелаза у звонастој области $(Oy\phi)$ равни, где је фракциони зарубљени радијус дуж одређеног правца дат као $y = R_j/R_i$, а фракциона виријална потенцијална енергија је $\phi = (E_{ji})_{\text{vir}}/(E_{ij})_{\text{vir}}$. Даље проучавање је посвећено расподелама масе описаних у раду Hernquist-a (1990) који даје профиле густине, за које може да се користи додатна релација да би се обрадио узорак од $N = 16$ елиптичних галаксија у $(Oy\phi)$ равни. Чак и када би еволуција елиптичних галаксија и халоа тамне материје у којима се оне налазе, у светлу овог модела, била карактерисана једнаким фракционим масама, m , и једнаким сразмерним радијусом зарубљености, или концентрације, $\Xi_u = R_u/r_u^\dagger$, $u = i, j$, она и даље не би могла да буде посматрана као стриктно хомологна, због различитих вредности фракционог радијуса зарубљености, y , или фракционог радијуса скалирања, $y^\dagger = r_j^\dagger/r_i^\dagger$, закључујући на основу објеката из узорка.